An increase in myocardial NAD(P)H oxidase activity has also been observed in human HF (33). By using mice lacking $p47^{phox}$ ($p47^{phox-/-}$ mice), Doerries et al. (20) demonstrated that a deficiency of the NAD(P)H oxidase protected the heart from LV remodeling and dysfunction after MI. Doughan et al. (21) provided the direct evidence that angiotensin II could mediate mitochondrial dysfunction via the activation of NAD(P)H oxidases in vascular endothelial cells. Angiotensin II increased mitochondrial ROS production, which was associated with decreased endothelial $NO^{\bullet}$ bioavailability. Therefore, among five Nox isoforms, Nox2 and Nox4 are the main isoforms in the diseased myocardium. Recent studies have demonstrated that Nox4, localized primarily within the mitochondria in cardiac myocytes, is responsible for enhanced ROS production and cardiac remodeling due to pressure overload and aging, thereby playing an important role in mediating cardiac dysfunction (2, 52). The role of Nox5 has not yet been clarified in HF.

Increased xanthine oxidase expression and activity were also reported in HF (11). Furthermore, LV contractile function and myocardial efficiency were improved by the treatment of HF animals with the xanthine oxidase inhibitor allopurinol (111). In addition, chronic treatment of animals following experimental MI with allopurinol significantly reduced adverse LV remodeling (68). These detrimental effects of xanthine oxidase might involve, at least in part, the inactivation of NO because it could reduce myocardial O_2 consumption and improve cardiac efficiency (50).

Uncoupled NOS can potentially lead to further ROS production via the oxidation of the essential NOS cofactor BH_4 (55). NOS3 [endothelial NOS (eNOS)] has been shown to be uncoupled and functionally important in cardiovascular pathological remodeling including HF (100). Under normal conditions, NOS3 consumes NADPH and generates NO and L-citrulline from L-arginine and O_2. When exposed to oxidative stress or when deprived of BH_4 or L-arginine, NOS3 becomes structurally unstable and generates ROS. It is unclear which cell type contributes mostly to ROS generated by NOS3 uncoupling. However, given that NOS3 is expressed in vascular endothelial cells and cardiac myocytes within the heart, these cells are well expected to be involved in this process. Uncoupled NOS3 has been shown to contribute to LV remodeling in response to chronic pressure overload in mice (99). Mice subjected to transverse thoracic aortic constriction had reduced BH_4 levels and uncoupling of eNOS in association with LV dilatation and contractile dysfunction, which could be partially inhibited by BH_4 treatment. In contrast, Ruetten et al. (85) reported that $eNOS^{-/-}$ mice subjected to aortic constriction developed worse contractile function, greater hypertrophy, and more interstitial fibrosis. Similarly, Scherrer-Crosbie et al. (89) reported that post-MI LV remodeling was more extensive in $eNOS^{-/-}$ mice. The reasons for these discrepant results remain unclear; however, it may be partly due to the opposing effects of NO and ROS derived from uncoupled NOS on cardiac hypertrophy and fibrosis.

Cytochrome *c* oxidase (COX), the terminal oxidase of the mitochondrial electron transport chain (complex IV), is composed of 13 subunits. The subunits COX I, II, and III are encoded by a single mitochondrial gene. COX I and II belong to the catalytic core, which is key for the assembly and the function of the complex. We have shown that the enzyme activity of electron transport chain complex I, III, and IV all decreased in mice subjected to MI (37). Wu et al. (115) also demonstrated that COX III overexpression resulted in a decreased abundance of COX I and a decrease in COX activity, accompanied by increased apoptosis in HF following MI.

The contribution of leukocytes has been suggested in the generation of ROS based on the findings that plasma levels of myeloperoxidase (MPO) correlated with the severity of HF and were independent predictors of outcomes in these patients (101). Plasma MPO indicates MPO mass in plasma as a marker of heightened leukocyte activation rather than systemic inflammation.

Oxidative Stress and Mitochondrial DNA Damage

ROS can damage mitochondrial macromolecules either at or near the site of their formation. Therefore, in addition to the role of mitochondria as a source of ROS, the mitochondria themselves can be damaged by ROS. Mitochondria have their own genomic system, mitochondrial DNA (mtDNA), a closed-circular double-stranded DNA molecule of ~16.5 kb. mtDNA contains 2 promoters, the light-strand (LSP) and heavy-strand promoters from which transcripts are produced and then processed to yield the individual mRNAs encoding 13 subunits of the oxidative phosphorylation, including 7 subunits (ND1, ND2, ND3, ND4, ND4L, ND5, and ND6) of rotenone-sensitive NADH-ubiquinone oxidoreductase (complex I), 1 subunit (cytochrome b) of ubiquinol-cytochrome *c* oxidoreductase (complex III) , 3 subunits (COI, COII, and COIII) of COX (complex IV), and 2 subunits (ATPases 6 and 8) of complex V along with 22 tRNAs and 2 rRNA (12S and 16S) subunits (4, 92). Transcription from the LSP also produces RNA primer, which is necessary for initiating mtDNA replication (Fig. 4) (14). Mitochondrial function is controlled by the mtDNA as well as by factors that regulate mtDNA transcription and/or replication such as mitochondrial transcription factor A (Fig. 4) (45).

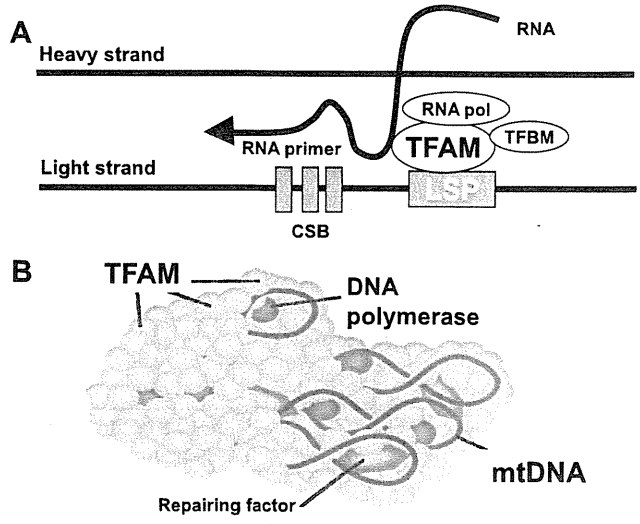

Fig. 4. Role of mitochondrial transcription factor A (TFAM) in mitochondrial DNA (mtDNA) replication (*A*) and maintenance (*B*). TFBM, mitochondrial transcription factor B; CSB, conserved sequence block; LSP, light-strand promoter.

The mtDNA could be a major target for ROS-mediated damage for several reasons. First, mitochondria do not have a complex chromatin organization consisting of histone proteins, which may serve as a protective barrier against ROS. Second, mtDNA has a limited repair activity against DNA damage. Third, a large part of $O_2^{\cdot -}$, formed inside the mitochondria, is unable to pass through the membranes and, hence, ROS damage occurs largely within the mitochondria. In fact, mtDNA accumulates significantly higher levels of the DNA oxidation product, 8-hydroxydeoxyguanosine, than nuclear DNA (26). As opposed to nuclear-encoded genes, mitochondrial-encoded gene expression is largely regulated by the copy number of mtDNA (113). Therefore, mitochondrial injury is reflected by mtDNA damage as well as by a decline in the mitochondrial RNA (mtRNA) transcripts, protein synthesis, and mitochondrial function (5).

Increased generation of ROS in the failing hearts was associated with mitochondrial damage and dysfunction, characterized by an increased lipid peroxidation in the mitochondria, a decreased mtDNA copy number, a decrease in the number of mtRNA transcripts, and a reduced oxidative capacity due to low complex enzyme activities (37). They thus can lead to a catastrophic cycle of mitochondrial functional decline, further ROS generation, and cellular injury. There is now a consensus view that the abnormalities in mtDNA replication/transcription as well as repair occur not only in a limited small subset of mitochondrial diseases but also in a more common form of HF phenotype such as post-MI and cardiomyopathy (40, 59, 64, 98, 108).

Oxidative Stress in Myocardial Remodeling

The tightly regulated production of relatively low levels of ROS is involved in modulating the activity of diverse intracellular molecules and signaling pathways, "redox signaling," with the potential to induce highly specific regulation in the cellular phenotype (Fig. 2) (22).

Alternatively, oxidative stress has direct effects on cellular structure and function and may activate integral signaling molecules in myocardial remodeling and failure (Fig. 5). Oxidative stress stimulates myocardial growth, matrix remodeling, and cellular dysfunction, which involve the activation of several downstream signaling pathways. First, ROS activate a broad variety of hypertrophy signaling kinases and transcription factors (86). ROS stimulate the tyrosine kinase Src, GTP-binding protein Ras, protein kinase C, mitogen-activated protein kinases (MAPK), and Jun-nuclear kinase (JNK). Low levels of H_2O_2 are associated with MAPK activation and protein synthesis, whereas higher levels stimulate MAPK, JNK, p38, and protein kinase B (Akt) kinases to induce apoptosis (53). Second, ROS induces apoptosis, another important contributor to remodeling and dysfunction, which is induced by ROS-mediated DNA and mitochondrial damage and activation of proapoptotic signaling kinases (12). Third, ROS cause DNA strand breaks, activating the nuclear enzyme poly(ADP-ribose) polymerase-1 (PARP-1). PARP-1 regulates the expression of a variety of inflammatory mediators, which facilitate the progression of cardiac remodeling. Fourth, ROS can activate MMPs, a family of proteolytic enzymes (97). MMPs are generally secreted in an inactive form and are activated posttranslationally by ROS from targeted interactions with critical cysteines in the propeptide autoinhibitory domain. ROS also stimulate transcription factors nuclear factor-κB, Ets, and activator protein-1 to stimulate MMP expression. MMPs play a pivotal role in normal tissue remodeling processes, such as cell migration, invasion, proliferation, and apoptosis. MMP activity has been shown to be increased in the failing hearts (16, 97). Furthermore, an MMP inhibitor can limit LV dilatation after an experimental MI (84). We have shown significant improvement in survival after MI in MMP-2 knockout mice, which was mainly attributable to the inhibition of early cardiac rupture and the development of subsequent LV remodeling and failure (32). Because MMP can be activated by ROS, one

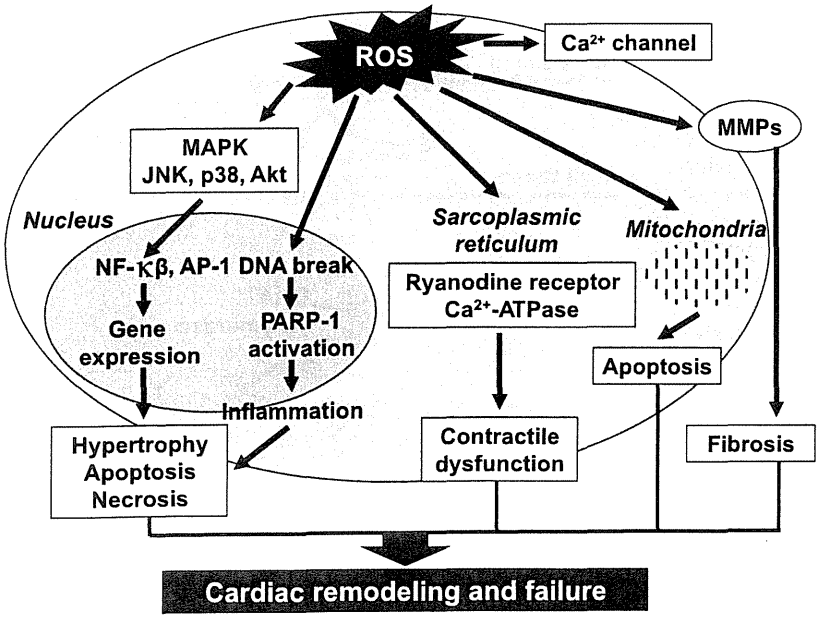

Fig. 5. Potential cellular and subcellular targets of oxidative stress relevant to heart failure (HF). MAPK, mitogen-activated protein kinases; JNK, Jun-nuclear kinase; PARP-1, poly(ADP-ribose) polymerase-1; MMPs, matrix metalloproteinases; AP-1, activator protein-1.

proposed mechanism of LV remodeling is the activation of MMPs secondary to increased ROS (82). Sustained MMP activation might influence the structural properties of the myocardium by providing an abnormal extracellular environment with which the myocytes interact. An $^{\bullet}OH$ scavenger, dimethylthiourea, inhibited the activation of MMP-2 in association with the development of LV remodeling and failure after MI (51). These findings raise the possibility that enhanced oxidative stress can be a stimulus for myocardial MMP activation, which plays an important role in the development and progression of HF. Finally, ROS directly influence contractile function by modifying proteins involved in excitation-contraction coupling (117). This includes modification of critical thiol groups (−SH) groups on the ryanodine receptor to enhance its open probability, the suppression of L-type calcium channel, and oxidative interaction with Ca^{2+} ATPase in the sarcoplasmic reticulum to inhibit Ca^{2+} uptake.

Oxidative Stress in Aging, Hypertension, and Diabetes Mellitus

Oxidative stress is highly relevant to aging and the development of various aging-related cardiovascular diseases, including HF. However, the involvement of specific forms of ROS and each antioxidant and/or ROS-producing enzymes in the process of aging remain obscure. Neither overexpression nor heterozygous knockout of mitochondrial SOD affected lifespan in mice (42, 112). In contrast, in transgenic mice overexpressing catalase in the mitochondria, maximal lifespan was extended by 20%, and aging-associated cardiac pathology was significantly delayed (90).

There is also substantial evidence that ROS generation is increased in hypertension (102). Moreover, the concomitant increase in myocardial ROS production was accompanied by the transition from compensated hypertrophy to failure in Dahl salt-sensitive rats fed by high-salt diet (106).

Insulin resistance and diabetes mellitus have been well known to adversely affect the development and progression of HF (41, 46). Indeed, the prevalence of diabetes in patients with HF is higher than in subjects without HF (15, 79). Diabetes mellitus often leads to HF, even in the absence of any other risk factors such as coronary artery disease or hypertension, suggesting that diabetes itself causes a specific form of cardiomyopathic state (8). It causes myocardial structural remodeling characterized by myocyte hypertrophy, interstitial fibrosis, and apoptosis (23), which increases cardiac muscle stiffness and may contribute to diastolic dysfunction. Diastolic dysfunction has been regarded as a hemodynamic hallmark in diabetes and ultimately contributes to the development of HF (1, 69).

A growing body of evidence suggests that the production of ROS is increased in the diabetic heart (43). Specifically, ROS are generated within the mitochondria from the diabetic heart (44). ROS impair prosurvival signaling pathways such as Akt in diabetic hearts and activates proinflammatory and cell death pathways such as NF-κB and the nuclear enzyme PARP-1, which in turn regulate the expression of proinflammatory cytokines, cell adhesion molecules, and inducible NOS (83). Overexpression of GSHPx could attenuate diastolic dysfunction, myocyte hypertrophy, and interstitial fibrosis in diabetic heart (65). These findings are consistent with previous studies demonstrating that ROS are involved in the structural alterations of the extracellular matrix collagens (72). Another important impact of diabetes mellitus in HF is the exacerbation of systolic dysfunction after MI. Previous clinical studies demonstrated that patients with diabetes had a worse outcome after MI than that without diabetes despite similar coronary patency and baseline LV function (27). Poor outcomes in patients with diabetes have been shown to be due to the progression of HF (3). Experimental studies demonstrated that hyperglycemia induced by streptozotocin exaggerates LV remodeling and failure after MI (93, 95). Similar to type 1 diabetes, LV remodeling and failure after MI were exacerbated also in high-fat diet-induced type 2 diabetes (66, 116).

Insulin resistance can occur as a consequence of HF (49, 76, 114). Patients with symptomatic dilated cardiomyopathy, excluding previously diagnosed type 2 diabetes, showed the abnormal response compared with healthy subjects by oral glucose tolerance tests (114) or the euglycemic-hyperinsulinemic clamp technique (49). Insulin resistance has been recognized also in several animal models of HF. Myocardial glucose uptake was decreased with the development of HF in a pacing-induced dog model (70, 71). Myocardial insulin resistance was due to the impairment of insulin signaling and associated with the decrease in ATP concentration. Liao et al. (60) demonstrated that the glucose tolerance was abnormal in mice with cardiac hypertrophy and HF due to pressure overload. Moreover, the control of postprandial hyperglycemia by α-glucosidase inhibitor could ameliorate cardiac hypertrophy and slow the progression to HF. These findings suggest that HF itself can cause insulin resistance, which may lead to the further exacerbation of HF.

Very little information has been available for the mechanisms responsible for the abnormalities in insulin signaling in the skeletal muscle from HF. Previous studies reported that serine phosphorylation of Akt was decreased in the skeletal

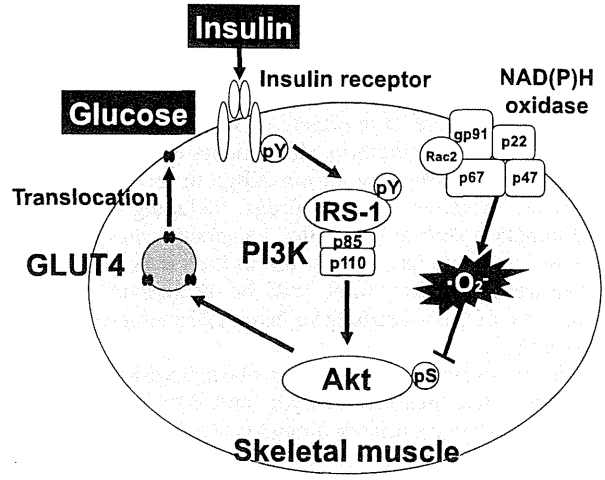

Fig. 6. Role of NAD(P)H oxidase-derived superoxide in the impairment of insulin signaling in the skeletal muscle. Insulin receptor, insulin receptor substrate-1 (IRS-1), phosphatidylinositol 3-kinase (PI3K), protein kinase B (Akt), and translocation of glucose transporter-4 (GLUT4) to plasma membrane from cytosol are involved in the insulin signaling in the skeletal muscle. Serine phosphorylation of Akt and GLUT4 translocation is impaired in insulin-stimulated skeletal muscle isolated from HF, which was consistent with the attenuation of changes in blood glucose after insulin load. NAD(P)H oxidase-derived superoxide impairs serine phosphorylation of Akt and GLUT4 translocation in the skeletal muscle with HF.

muscle from a HF model of post-MI (91). Another report showed that serine phosphorylation of Akt and glucose transporter-4 (GLUT4) translocation was decreased in the myocardial tissue from a pacing-induced HF model (71). The similar impairment of insulin signaling was observed in both heart and skeletal muscle obtained from HF, indicating that systemic factors may be involved for this abnormality. We recently found that whole body insulin resistance was induced in a murine HF model of post-MI, which was accompanied by the impaired insulin signaling in the skeletal muscle, specifically the decreases in serine phosphorylation of Akt and GLUT4 translocation (Fig. 6) (73). Importantly, NAD(P)H oxidase inhibitor significantly ameliorated insulin resistance as well as the impaired insulin signaling in the skeletal muscle. ROS production via NAD(P)H oxidase leads to the impairment of insulin signaling and glucose uptake in the skeletal muscle also in type 2 diabetes (96).

Clinical Perspectives

There were clinical studies reported that examined the effects of various antioxidants on HF (87). The vitamin antioxidants α-tocopherol (vitamin E) and ascorbic acid (vitamin C) scavenge ROS and prevent free radical chain reactions and have been studied extensively in HF. α-Tocopherol levels were decreased, and dietary supplements of α-tocopherol exerted a therapeutic effect in animal models of HF (17). Short-term vitamin E supplementation reduced the levels of oxidative stress biomarkers also in patients with HF (25). However, no significant effects were proved on symptoms or clinical outcomes (48). Moreover, large-scale clinical trials reported that the long-term supplementation of vitamin E exerted no effects on primary prevention of cardiovascular events and was even associated with increased risk of developing HF (61, 63).

Xanthine oxidase inhibition with allopurinol is expected to be beneficial based on the findings that uric acid, the product of xanthine oxidoreductase, was increased in the failing human heart and was associated with poor outcomes (28). In fact, xanthine oxidase inhibition with allopurinol has been shown to improve endothelial as well as cardiac function in HF (13, 19). However, there were little effects of xanthine oxidase inhibition on clinical endpoints in HF patients except for modest improvement in symptoms in the subgroup of increased uric acid levels. Moreover, various drugs, including ACE inhibitors, β-blockers such as carvedilol, and statins, may directly or indirectly modulate oxidative stress in the cardiovascular system. However, further work will be needed to determine whether any of these drugs have beneficial therapeutic effects on human HF.

Oxidative stress markers such as plasma-oxidized low-density lipoproteins, malondialdehyde and MPO (an index of leukocyte activation), urinary biopyrrins (oxidative metabolites of bilirubin), and plasma and urine isoprostane levels are expected to provide important information regarding the pathogenesis of HF or the identification of subjects at risk for HF, the future risk stratification, the diagnosis, or monitoring therapy of HF as biomarkers (10).

Conclusion

To improve the prognosis of patients with HF, we need to develop therapeutic strategies based on a novel insight into the pathophysiology of HF. The approach of regulating oxidative stress in the heart as well as in the skeletal muscle may contribute to establish the effective treatment strategies against HF. Therefore, therapeutic strategies to modulate this maladaptive response should become a target for future extensive investigation.

GRANTS

The work presented in this article was supported in part by grants from the Ministry of Education, Science, and Culture, Japan (nos. 12670676, 14370230, 17390223, 17659223, 20117004, and 21390236); Health Sciences Research Grants from the Japanese Ministry of Health, Labor, and Welfare (Comprehensive Research on Cardiovascular Diseases); and the Japan Heart Foundation.

DISCLOSURES

Conflict of interest: none declared.

REFERENCES

1. **Abe T, Ohga Y, Tabayashi N, Kobayashi S, Sakata S, Misawa H, Tsuji T, Kohzuki H, Suga H, Taniguchi S, Takaki M.** Left ventricular diastolic dysfunction in type 2 diabetes mellitus model rats. *Am J Physiol Heart Circ Physiol* 282: H138–H148, 2002.
2. **Ago T, Kuroda J, Pain J, Fu C, Li H, Sadoshima J.** Upregulation of Nox4 by hypertrophic stimuli promotes apoptosis and mitochondrial dysfunction in cardiac myocytes. *Circ Res* 106: 1253–1264, 2010.
3. **Aguilar D, Solomon SD, Kober L, Rouleau JL, Skali H, McMurray JJ, Francis GS, Henis M, O'Connor CM, Diaz R, Belenkov YN, Varshavsky S, Leimberger JD, Velazquez EJ, Califf RM, Pfeffer MA.** Newly diagnosed and previously known diabetes mellitus and 1-year outcomes of acute myocardial infarction: the VALsartan In Acute myocardial iNfarcTion (VALIANT) trial. *Circulation* 110: 1572–1578, 2004.
4. **Attardi G, Schatz G.** Biogenesis of mitochondria. *Annu Rev Cell Biol* 4: 289–333, 1988.
5. **Ballinger SW, Patterson C, Yan CN, Doan R, Burow DL, Young CG, Yakes FM, Van Houten B, Ballinger CA, Freeman BA, Runge MS.** Hydrogen peroxide- and peroxynitrite-induced mitochondrial DNA damage and dysfunction in vascular endothelial and smooth muscle cells. *Circ Res* 86: 960–966, 2000.
7. **Bauersachs J, Bouloumie A, Fraccarollo D, Hu K, Busse R, Ertl G.** Endothelial dysfunction in chronic myocardial infarction despite increased vascular endothelial nitric oxide synthase and soluble guanylate cyclase expression: role of enhanced vascular superoxide production. *Circulation* 100: 292–298, 1999.
8. **Beckman JA, Creager MA, Libby P.** Diabetes and atherosclerosis: epidemiology, pathophysiology, and management. *JAMA* 287: 2570–2581, 2002.
9. **Belch JJ, Bridges AB, Scott N, Chopra M.** Oxygen free radicals and congestive heart failure. *Br Heart J* 65: 245–248, 1991.
10. **Braunwald E.** Biomarkers in heart failure. *N Engl J Med* 358: 2148–2159, 2008.
11. **Cappola TP, Kass DA, Nelson GS, Berger RD, Rosas GO, Kobeissi ZA, Marban E, Hare JM.** Allopurinol improves myocardial efficiency in patients with idiopathic dilated cardiomyopathy. *Circulation* 104: 2407–2411, 2001.
12. **Cesselli D, Jakoniuk I, Barlucchi L, Beltrami AP, Hintze TH, Nadal-Ginard B, Kajstura J, Leri A, Anversa P.** Oxidative stress-mediated cardiac cell death is a major determinant of ventricular dysfunction and failure in dog dilated cardiomyopathy. *Circ Res* 89: 279–286, 2001.
13. **Cingolani HE, Plastino JA, Escudero EM, Mangal B, Brown J, Perez NG.** The effect of xanthine oxidase inhibition upon ejection fraction in heart failure patients: La Plata Study. *J Card Fail* 12: 491–498, 2006.
14. **Clayton DA.** Replication and transcription of vertebrate mitochondrial DNA. *Annu Rev Cell Biol* 7: 453–478, 1991.
15. **Cohn JN, Tognoni G.** A randomized trial of the angiotensin-receptor blocker valsartan in chronic heart failure. *N Engl J Med* 345: 1667–1675, 2001.

15a. **CONSENSUS Trial Study Group.** Effects of enalapril on mortality in severe congestive heart failure. Results of the Cooperative North Scan-

dinavian Enalapril Survival Study (CONSENSUS). *N Engl J Med* 316: 1429–1435, 1987.

16. **Creemers EE, Cleutjens JP, Smits JF, Daemen MJ.** Matrix metalloproteinase inhibition after myocardial infarction: a new approach to prevent heart failure? *Circ Res* 89: 201–210, 2001.
17. **Dhalla AK, Hill MF, Singal PK.** Role of oxidative stress in transition of hypertrophy to heart failure. *J Am Coll Cardiol* 28: 506–514, 1996.
18. **Dickstein K, Cohen-Solal A, Filippatos G, McMurray JJ, Ponikowski P, Poole-Wilson PA, Stromberg A, van Veldhuisen DJ, Atar D, Hoes AW, Keren A, Mebazaa A, Nieminen M, Priori SG, Swedberg K.** ESC guidelines for the diagnosis and treatment of acute and chronic heart failure 2008: the Task Force for the diagnosis and treatment of acute and chronic heart failure 2008 of the European Society of Cardiology. Developed in collaboration with the Heart Failure Association of the ESC (HFA) and endorsed by the European Society of Intensive Care Medicine (ESICM). *Eur J Heart Fail* 10: 933–989, 2008.
19. **Doehner W, Schoene N, Rauchhaus M, Leyva-Leon F, Pavitt DV, Reaveley DA, Schuler G, Coats AJ, Anker SD, Hambrecht R.** Effects of xanthine oxidase inhibition with allopurinol on endothelial function and peripheral blood flow in hyperuricemic patients with chronic heart failure: results from 2 placebo-controlled studies. *Circulation* 105: 2619–2624, 2002.
20. **Doerries C, Grote K, Hilfiker-Kleiner D, Luchtefeld M, Schaefer A, Holland SM, Sorrentino S, Manes C, Schieffer B, Drexler H, Landmesser U.** Critical role of the NAD(P)H oxidase subunit p47phox for left ventricular remodeling/dysfunction and survival after myocardial infarction. *Circ Res* 100: 894–903, 2007.
21. **Doughan AK, Harrison DG, Dikalov SI.** Molecular mechanisms of angiotensin II-mediated mitochondrial dysfunction: linking mitochondrial oxidative damage and vascular endothelial dysfunction. *Circ Res* 102: 488–496, 2008.
22. **Finkel T.** Oxidant signals and oxidative stress. *Curr Opin Cell Biol* 15: 247–254, 2003.
23. **Fiordaliso F, Li B, Latini R, Sonnenblick EH, Anversa P, Leri A, Kajstura J.** Myocyte death in streptozotocin-induced diabetes in rats in angiotensin II- dependent. *Lab Invest* 80: 513–527, 2000.
24. **Gajarsa JJ, Kloner RA.** Left ventricular remodeling in the post-infarction heart: a review of cellular, molecular mechanisms, and therapeutic modalities. *Heart Fail Rev* 16: 13–21, 2011.
25. **Ghatak A, Brar MJ, Agarwal A, Goel N, Rastogi AK, Vaish AK, Sircar AR, Chandra M.** Oxy free radical system in heart failure and therapeutic role of oral vitamin E. *Int J Cardiol* 57: 119–127, 1996.
26. **Giulivi C, Boveris A, Cadenas E.** Hydroxyl radical generation during mitochondrial electron transfer and the formation of 8-hydroxydesoxyguanosine in mitochondrial DNA. *Arch Biochem Biophys* 316: 909–916, 1995.
27. **Haffner SM, Lehto S, Ronnemaa T, Pyorala K, Laakso M.** Mortality from coronary heart disease in subjects with type 2 diabetes and in nondiabetic subjects with and without prior myocardial infarction. *N Engl J Med* 339: 229–234, 1998.
28. **Hamaguchi S, Furumoto T, Tsuchihashi-Makaya M, Goto K, Goto D, Yokota T, Kinugawa S, Yokoshiki H, Takeshita A, Tsutsui H.** Hyperuricemia predicts adverse outcomes in patients with heart failure. *Int J Cardiol* 151: 142–147, 2011.
29. **Hamaguchi S, Kinugawa S, Tsuchihashi-Makaya M, Goto K, Goto D, Yokota T, Yamada S, Yokoshiki H, Takeshita A, Tsutsui H.** Spironolactone use at discharge was associated with improved survival in hospitalized patients with systolic heart failure. *Am Heart J* 160: 1156–1162, 2010.
30. **Hamaguchi S, Tsuchihashi-Makaya M, Kinugawa S, Goto D, Yokota T, Goto K, Yamada S, Yokoshiki H, Takeshita A, Tsutsui H.** Body mass index is an independent predictor of long-term outcomes in patients hospitalized with heart failure in Japan. *Circ J* 74: 2605–2611, 2010.
31. **Hamaguchi S, Tsuchihashi-Makaya M, Kinugawa S, Yokota T, Ide T, Takeshita A, Tsutsui H.** Chronic kidney disease as an independent risk for long-term adverse outcomes in patients hospitalized with heart failure in Japan. Report from the Japanese Cardiac Registry of Heart Failure in Cardiology (JCARE-CARD). *Circ J* 73: 1442–1447, 2009.
32. **Hayashidani S, Tsutsui H, Ikeuchi M, Shiomi T, Matsusaka H, Kubota T, Imanaka-Yoshida K, Itoh T, Takeshita A.** Targeted deletion of MMP-2 attenuates early LV rupture and late remodeling after experimental myocardial infarction. *Am J Physiol Heart Circ Physiol* 285: H1229–H1235, 2003.
33. **Heymes C, Bendall JK, Ratajczak P, Cave AC, Samuel JL, Hasenfuss G, Shah AM.** Increased myocardial NADPH oxidase activity in human heart failure. *J Am Coll Cardiol* 41: 2164–2171, 2003.
34. **Hill MF, Singal PK.** Antioxidant and oxidative stress changes during heart failure subsequent to myocardial infarction in rats. *Am J Pathol* 148: 291–300, 1996.
35. **Hill MF, Singal PK.** Right and left myocardial antioxidant responses during heart failure subsequent to myocardial infarction. *Circulation* 96: 2414–2420, 1997.
36. **Hunt SA, Abraham WT, Chin MH, Feldman AM, Francis GS, Ganiats TG, Jessup M, Konstam MA, Mancini DM, Michl K, Oates JA, Rahko PS, Silver MA, Stevenson LW, Yancy CW.** 2009 focused update incorporated into the ACC/AHA 2005 Guidelines for the Diagnosis and Management of Heart Failure in Adults: a report of the American College of Cardiology Foundation/American Heart Association Task Force on Practice Guidelines: developed in collaboration with the International Society for Heart and Lung Transplantation. *Circulation* 119: e391–e479, 2009.
37. **Ide T, Tsutsui H, Hayashidani S, Kang D, Suematsu N, Nakamura K, Utsumi H, Hamasaki N, Takeshita A.** Mitochondrial DNA damage and dysfunction associated with oxidative stress in failing hearts after myocardial infarction. *Circ Res* 88: 529–535, 2001.
38. **Ide T, Tsutsui H, Kinugawa S, Suematsu N, Hayashidani S, Ichikawa K, Utsumi H, Machida Y, Egashira K, Takeshita A.** Direct evidence for increased hydroxyl radicals originating from superoxide in the failing myocardium. *Circ Res* 86: 152–157, 2000.
39. **Ide T, Tsutsui H, Kinugawa S, Utsumi H, Kang D, Hattori N, Uchida K, Arimura K, Egashira K, Takeshita A.** Mitochondrial electron transport complex I is a potential source of oxygen free radicals in the failing myocardium. *Circ Res* 85: 357–363, 1999.
40. **Ikeuchi M, Matsusaka H, Kang D, Matsushima S, Ide T, Kubota T, Fujiwara T, Hamasaki N, Takeshita A, Sunagawa K, Tsutsui H.** Overexpression of mitochondrial transcription factor a ameliorates mitochondrial deficiencies and cardiac failure after myocardial infarction. *Circulation* 112: 683–690, 2005.
41. **Ingelsson E, Sundstrom J, Arnlov J, Zethelius B, Lind L.** Insulin resistance and risk of congestive heart failure. *JAMA* 294: 334–341, 2005.
42. **Jang YC, Perez VI, Song W, Lustgarten MS, Salmon AB, Mele J, Qi W, Liu Y, Liang H, Chaudhuri A, Ikeno Y, Epstein CJ, Van Remmen H, Richardson A.** Overexpression of Mn superoxide dismutase does not increase life span in mice. *J Gerontol A Biol Sci Med Sci* 64: 1114–1125, 2009.
43. **Kakkar R, Kalra J, Mantha SV, Prasad K.** Lipid peroxidation and activity of antioxidant enzymes in diabetic rats. *Mol Cell Biochem* 151: 113–119, 1995.
44. **Kanazawa A, Nishio Y, Kashiwagi A, Inagaki H, Kikkawa R, Horiike K.** Reduced activity of mtTFA decreases the transcription in mitochondria isolated from diabetic rat heart. *Am J Physiol Endocrinol Metab* 282: E778–E785, 2002.
45. **Kang D, Hamasaki N.** Mitochondrial transcription factor A in the maintenance of mitochondrial DNA: overview of its multiple roles. *Ann NY Acad Sci* 1042: 101–108, 2005.
46. **Kannel WB, McGee DL.** Diabetes and cardiovascular disease. The Framingham study. *JAMA* 241: 2035–2038, 1979.
47. **Katz SD, Hryniewicz K, Hriljac I, Balidemaj K, Dimayuga C, Hudaihed A, Yasskiy A.** Vascular endothelial dysfunction and mortality risk in patients with chronic heart failure. *Circulation* 111: 310–314, 2005.
48. **Keith ME, Jeejeebhoy KN, Langer A, Kurian R, Barr A, O'Kelly B, Sole MJ.** A controlled clinical trial of vitamin E supplementation in patients with congestive heart failure. *Am J Clin Nutr* 73: 219–224, 2001.
49. **Kemppainen J, Tsuchida H, Stolen K, Karlsson H, Bjornholm M, Heinonen OJ, Nuutila P, Krook A, Knuuti J, Zierath JR.** Insulin signalling and resistance in patients with chronic heart failure. *J Physiol* 550: 305–315, 2003.
50. **Kinugawa S, Huang H, Wang Z, Kaminski PM, Wolin MS, Hintze TH.** A defect of neuronal nitric oxide synthase increases xanthine oxidase-derived superoxide anion and attenuates the control of myocardial oxygen consumption by nitric oxide derived from endothelial nitric oxide synthase. *Circ Res* 96: 355–362, 2005.
51. **Kinugawa S, Tsutsui H, Hayashidani S, Ide T, Suematsu N, Satoh S, Utsumi H, Takeshita A.** Treatment with dimethylthiourea prevents left

ventricular remodeling and failure after experimental myocardial infarction in mice: role of oxidative stress. *Circ Res* 87: 392–398, 2000.

52. **Kuroda J, Ago T, Matsushima S, Zhai P, Schneider MD, Sadoshima J.** NADPH oxidase 4 (Nox4) is a major source of oxidative stress in the failing heart. *Proc Natl Acad Sci USA* 107: 15565–15570, 2010.
53. **Kwon SH, Pimentel DR, Remondino A, Sawyer DB, Colucci WS.** H(2)O(2) regulates cardiac myocyte phenotype via concentration-dependent activation of distinct kinase pathways. *J Mol Cell Cardiol* 35: 615–621, 2003.
54. **Lambeth JD.** NOX enzymes and the biology of reactive oxygen. *Nat Rev Immunol* 4: 181–189, 2004.
55. **Landmesser U, Dikalov S, Price SR, McCann L, Fukai T, Holland SM, Mitch WE, Harrison DG.** Oxidation of tetrahydrobiopterin leads to uncoupling of endothelial cell nitric oxide synthase in hypertension. *J Clin Invest* 111: 1201–1209, 2003.
56. **Landmesser U, Drexler H.** The clinical significance of endothelial dysfunction. *Curr Opin Cardiol* 20: 547–551, 2005.
57. **Le CT, Hollaar L, van der Valk EJ, van der Laarse A.** Buthionine sulfoximine reduces the protective capacity of myocytes to withstand peroxide-derived free radical attack. *J Mol Cell Cardiol* 25: 519–528, 1993.
58. **Li JM, Shah AM.** Mechanism of endothelial cell NADPH oxidase activation by angiotensin II. Role of the p47phox subunit. *J Biol Chem* 278: 12094–12100, 2003.
59. **Li YY, Chen D, Watkins SC, Feldman AM.** Mitochondrial abnormalities in tumor necrosis factor-alpha-induced heart failure are associated with impaired DNA repair activity. *Circulation* 104: 2492–2497, 2001.
60. **Liao Y, Takashima S, Zhao H, Asano Y, Shintani Y, Minamino T, Kim J, Fujita M, Hori M, Kitakaze M.** Control of plasma glucose with alpha-glucosidase inhibitor attenuates oxidative stress and slows the progression of heart failure in mice. *Cardiovasc Res* 70: 107–116, 2006.
61. **Lonn E, Bosch J, Yusuf S, Sheridan P, Pogue J, Arnold JM, Ross C, Arnold A, Sleight P, Probstfield J, Dagenais GR.** Effects of long-term vitamin E supplementation on cardiovascular events and cancer: a randomized controlled trial. *JAMA* 293: 1338–1347, 2005.
62. **Mallat Z, Philip I, Lebret M, Chatel D, Maclouf J, Tedgui A.** Elevated levels of 8-iso-prostaglandin F2alpha in pericardial fluid of patients with heart failure: a potential role for in vivo oxidant stress in ventricular dilatation and progression to heart failure. *Circulation* 97: 1536–1539, 1998.
63. **Marchioli R, Levantesi G, Macchia A, Marfisi RM, Nicolosi GL, Tavazzi L, Tognoni G, Valagussa F.** Vitamin E increases the risk of developing heart failure after myocardial infarction: Results from the GISSI-Prevenzione trial. *J Cardiovasc Med (Hagerstown)* 7: 347–350, 2006.
64. **Matsushima S, Ide T, Yamato M, Matsusaka H, Hattori F, Ikeuchi M, Kubota T, Sunagawa K, Hasegawa Y, Kurihara T, Oikawa S, Kinugawa S, Tsutsui H.** Overexpression of mitochondrial peroxiredoxin-3 prevents left ventricular remodeling and failure after myocardial infarction in mice. *Circulation* 113: 1779–1786, 2006.
65. **Matsushima S, Kinugawa S, Ide T, Matsusaka H, Inoue N, Ohta Y, Yokota T, Sunagawa K, Tsutsui H.** Overexpression of glutathione peroxidase attenuates myocardial remodeling and preserves diastolic function in diabetic heart. *Am J Physiol Heart Circ Physiol* 291: H2237–H2245, 2006.
66. **Matsushima S, Kinugawa S, Yokota T, Inoue N, Ohta Y, Hamaguchi S, Tsutsui H.** Increased myocardial NAD(P)H oxidase-derived superoxide causes the exacerbation of postinfarct heart failure in type 2 diabetes. *Am J Physiol Heart Circ Physiol* 297: H409–H416, 2009.
67. **McMurray JJ.** Clinical practice. Systolic heart failure. *N Engl J Med* 362: 228–238, 2010.
68. **Minhas KM, Saraiva RM, Schuleri KH, Lehrke S, Zheng M, Saliaris AP, Berry CE, Barouch LA, Vandegaer KM, Li D, Hare JM.** Xanthine oxidoreductase inhibition causes reverse remodeling in rats with dilated cardiomyopathy. *Circ Res* 98: 271–279, 2006.
69. **Mizushige K, Yao L, Noma T, Kiyomoto H, Yu Y, Hosomi N, Ohmori K, Matsuo H.** Alteration in left ventricular diastolic filling and accumulation of myocardial collagen at insulin-resistant prediabetic stage of a type II diabetic rat model. *Circulation* 101: 899–907, 2000.
70. **Nikolaidis LA, Elahi D, Hentosz T, Doverspike A, Huerbin R, Zourelias L, Stolarski C, Shen YT, Shannon RP.** Recombinant glucagon-like peptide-1 increases myocardial glucose uptake and improves left ventricular performance in conscious dogs with pacing-induced dilated cardiomyopathy. *Circulation* 110: 955–961, 2004.
71. **Nikolaidis LA, Sturzu A, Stolarski C, Elahi D, Shen YT, Shannon RP.** The development of myocardial insulin resistance in conscious dogs with advanced dilated cardiomyopathy. *Cardiovasc Res* 61: 297–306, 2004.
72. **Norton GR, Candy G, Woodiwiss AJ.** Aminoguanidine prevents the decreased myocardial compliance produced by streptozotocin-induced diabetes mellitus in rats. *Circulation* 93: 1905–1912, 1996.
73. **Ohta Y, Kinugawa S, Matsushima S, Ono T, Sobirin MA, Inoue N, Yokota T, Hirabayashi K, Tsutsui H.** Oxidative stress impairs insulin signal in skeletal muscle and causes insulin resistance in post-infarct heart failure. *Am J Physiol Heart Circ Physiol* 300: H1637–H1644, 2011.
74. **Pacher P, Beckman JS, Liaudet L.** Nitric oxide and peroxynitrite in health and disease. *Physiol Rev* 87: 315–424, 2007.
75. **Packer M, Coats AJ, Fowler MB, Katus HA, Krum H, Mohacsi P, Rouleau JL, Tendera M, Castaigne A, Roecker EB, Schultz MK, DeMets DL.** Effect of carvedilol on survival in severe chronic heart failure. *N Engl J Med* 344: 1651–1658, 2001.
76. **Paolisso G, Tagliamonte MR, Rizzo MR, Gambardella A, Gualdiero P, Lama D, Varricchio G, Gentile S, Varricchio M.** Prognostic importance of insulin-mediated glucose uptake in aged patients with congestive heart failure secondary to mitral and/or aortic valve disease. *Am J Cardiol* 83: 1338–1344, 1999.
77. **Perrelli MG, Pagliaro P, Penna C.** Ischemia/reperfusion injury and cardioprotective mechanisms: Role of mitochondria and reactive oxygen species. *World J Cardiol* 3: 186–200, 2011.
78. **Pfeffer JM, Pfeffer MA, Fletcher PJ, Braunwald E.** Progressive ventricular remodeling in rat with myocardial infarction. *Am J Physiol Heart Circ Physiol* 260: H1406–H1414, 1991.
79. **Pfeffer MA, Swedberg K, Granger CB, Held P, McMurray JJ, Michelson EL, Olofsson B, Ostergren J, Yusuf S, Pocock S.** Effects of candesartan on mortality and morbidity in patients with chronic heart failure: the CHARM-Overall programme. *Lancet* 362: 759–766, 2003.
80. **Pitt B, Poole-Wilson PA, Segal R, Martinez FA, Dickstein K, Camm AJ, Konstam MA, Riegger G, Klinger GH, Neaton J, Sharma D, Thiyagarajan B.** Effect of losartan compared with captopril on mortality in patients with symptomatic heart failure: randomised trial–the Losartan Heart Failure Survival Study ELITE II. *Lancet* 355: 1582–1587, 2000.
81. **Pitt B, Zannad F, Remme WJ, Cody R, Castaigne A, Perez A, Palensky J, Wittes J.** The effect of spironolactone on morbidity and mortality in patients with severe heart failure. Randomized Aldactone Evaluation Study Investigators. *N Engl J Med* 341: 709–717, 1999.
82. **Rajagopalan S, Meng XP, Ramasamy S, Harrison DG, Galis ZS.** Reactive oxygen species produced by macrophage-derived foam cells regulate the activity of vascular matrix metalloproteinases in vitro. Implications for atherosclerotic plaque stability. *J Clin Invest* 98: 2572–2579, 1996.
83. **Rajesh M, Mukhopadhyay P, Batkai S, Patel V, Saito K, Matsumoto S, Kashiwaya Y, Horvath B, Mukhopadhyay B, Becker L, Hasko G, Liaudet L, Wink DA, Veves A, Mechoulam R, Pacher P.** Cannabidiol attenuates cardiac dysfunction, oxidative stress, fibrosis, and inflammatory and cell death signaling pathways in diabetic cardiomyopathy. *J Am Coll Cardiol* 56: 2115–2125, 2010.
84. **Rohde LE, Ducharme A, Arroyo LH, Aikawa M, Sukhova GH, Lopez-Anaya A, McClure KF, Mitchell PG, Libby P, Lee RT.** Matrix metalloproteinase inhibition attenuates early left ventricular enlargement after experimental myocardial infarction in mice. *Circulation* 99: 3063–3070, 1999.
85. **Ruetten H, Dimmeler S, Gehring D, Ihling C, Zeiher AM.** Concentric left ventricular remodeling in endothelial nitric oxide synthase knockout mice by chronic pressure overload. *Cardiovasc Res* 66: 444–453, 2005.
86. **Sabri A, Hughie HH, Lucchesi PA.** Regulation of hypertrophic and apoptotic signaling pathways by reactive oxygen species in cardiac myocytes. *Antioxid Redox Signal* 5: 731–740, 2003.
87. **Sawyer DB.** Oxidative stress in heart failure: what are we missing? *Am J Med Sci* 342: 120–124, 2011.
88. **Sawyer DB, Colucci WS.** Mitochondrial oxidative stress in heart failure: "oxygen wastage" revisited. *Circ Res* 86: 119–120, 2000.
89. **Scherrer-Crosbie M, Ullrich R, Bloch KD, Nakajima H, Nasseri B, Aretz HT, Lindsey ML, Vancon AC, Huang PL, Lee RT, Zapol WM, Picard MH.** Endothelial nitric oxide synthase limits left ventricular remodeling after myocardial infarction in mice. *Circulation* 104: 1286–1291, 2001.
90. **Schriner SE, Linford NJ, Martin GM, Treuting P, Ogburn CE, Emond M, Coskun PE, Ladiges W, Wolf N, Van Remmen H,**

Wallace DC, Rabinovitch PS. Extension of murine life span by overexpression of catalase targeted to mitochondria. *Science* 308: 1909–1911, 2005.

91. **Schulze PC, Fang J, Kassik KA, Gannon J, Cupesi M, MacGillivray C, Lee RT, Rosenthal N.** Transgenic overexpression of locally acting insulin-like growth factor-1 inhibits ubiquitin-mediated muscle atrophy in chronic left-ventricular dysfunction. *Circ Res* 97: 418–426, 2005.
92. **Shadel GS, Clayton DA.** Mitochondrial DNA maintenance in vertebrates. *Annu Rev Biochem* 66: 409–435, 1997.
93. **Shiomi T, Tsutsui H, Ikeuchi M, Matsusaka H, Hayashidani S, Suematsu N, Wen J, Kubota T, Takeshita A.** Streptozotocin-induced hyperglycemia exacerbates left ventricular remodeling and failure after experimental myocardial infarction. *J Am Coll Cardiol* 42: 165–172, 2003.
94. **Shiomi T, Tsutsui H, Matsusaka H, Murakami K, Hayashidani S, Ikeuchi M, Wen J, Kubota T, Utsumi H, Takeshita A.** Overexpression of glutathione peroxidase prevents left ventricular remodeling and failure after myocardial infarction in mice. *Circulation* 109: 544–549, 2004.
95. **Smith HM, Hamblin M, Hill MF.** Greater propensity of diabetic myocardium for oxidative stress after myocardial infarction is associated with the development of heart failure. *J Mol Cell Cardiol* 39: 657–665, 2005.
96. **Sowers JR.** Insulin resistance and hypertension. *Am J Physiol Heart Circ Physiol* 286: H1597–H1602, 2004.
97. **Spinale FG, Coker ML, Thomas CV, Walker JD, Mukherjee R, Hebbar L.** Time-dependent changes in matrix metalloproteinase activity and expression during the progression of congestive heart failure: relation to ventricular and myocyte function. *Circ Res* 82: 482–495, 1998.
98. **Suematsu N, Tsutsui H, Wen J, Kang D, Ikeuchi M, Ide T, Hayashidani S, Shiomi T, Kubota T, Hamasaki N, Takeshita A.** Oxidative stress mediates tumor necrosis factor-alpha-induced mitochondrial DNA damage and dysfunction in cardiac myocytes. *Circulation* 107: 1418–1423, 2003.
99. **Takimoto E, Champion HC, Li M, Ren S, Rodriguez ER, Tavazzi B, Lazzarino G, Paolocci N, Gabrielson KL, Wang Y, Kass DA.** Oxidant stress from nitric oxide synthase-3 uncoupling stimulates cardiac pathologic remodeling from chronic pressure load. *J Clin Invest* 115: 1221–1231, 2005.
100. **Takimoto E, Kass DA.** Role of oxidative stress in cardiac hypertrophy and remodeling. *Hypertension* 49: 241–248, 2007.
101. **Tang WH, Tong W, Troughton RW, Martin MG, Shrestha K, Borowski A, Jasper S, Hazen SL, Klein AL.** Prognostic value and echocardiographic determinants of plasma myeloperoxidase levels in chronic heart failure. *J Am Coll Cardiol* 49: 2364–2370, 2007.
102. **Touyz RM, Briones AM.** Reactive oxygen species and vascular biology: implications in human hypertension. *Hypertens Res* 34: 5–14, 2011.
103. **Tsuchihashi-Makaya M, Furumoto T, Kinugawa S, Hamaguchi S, Goto K, Goto D, Yamada S, Yokoshiki H, Takeshita A, Tsutsui H.** Discharge use of angiotensin receptor blockers provides comparable effects with angiotensin-converting enzyme inhibitors on outcomes in patients hospitalized for heart failure. *Hypertens Res* 33: 197–202, 2010.
104. **Tsuchihashi-Makaya M, Hamaguchi S, Kinugawa S, Yokota T, Goto D, Yokoshiki H, Kato N, Takeshita A, Tsutsui H.** Characteristics and outcomes of hospitalized patients with heart failure and reduced vs preserved ejection fraction. Report from the Japanese Cardiac Registry of Heart Failure in Cardiology (JCARE-CARD). *Circ J* 73: 1893–1900, 2009.
105. **Tsuchihashi-Makaya M, Kinugawa S, Yokoshiki H, Hamaguchi S, Yokota T, Goto D, Goto K, Takeshita A, Tsutsui H.** Beta-blocker use at discharge in patients hospitalized for heart failure is associated with improved survival. *Circ J* 74: 1364–1371, 2010.
106. **Tsutsui H, Ide T, Hayashidani S, Kinugawa S, Suematsu N, Utsumi H, Takeshita A.** Effects of ACE inhibition on left ventricular failure and oxidative stress in Dahl salt-sensitive rats. *J Cardiovasc Pharmacol* 37: 725–733, 2001.
107. **Tsutsui H, Ide T, Hayashidani S, Suematsu N, Utsumi H, Nakamura R, Egashira K, Takeshita A.** Greater susceptibility of failing cardiac myocytes to oxygen free radical-mediated injury. *Cardiovasc Res* 49: 103–109, 2001.
108. **Tsutsui H, Ide T, Shiomi T, Kang D, Hayashidani S, Suematsu N, Wen J, Utsumi H, Hamasaki N, Takeshita A.** 8-oxo-dGTPase, which prevents oxidative stress-induced DNA damage, increases in the mitochondria from failing hearts. *Circulation* 104: 2883–2885, 2001.
109. **Tsutsui H, Tsuchihashi-Makaya M, Kinugawa S, Goto D, Takeshita A.** Characteristics and outcomes of patients with heart failure in general practices and hospitals. *Circ J* 71: 449–454, 2007.
110. **Tsutsui H, Tsuchihashi-Makaya M, Kinugawa S, Goto D, Takeshita A.** Clinical characteristics and outcome of hospitalized patients with heart failure in Japan. *Circ J* 70: 1617–1623, 2006.
111. **Ukai T, Cheng CP, Tachibana H, Igawa A, Zhang ZS, Cheng HJ, Little WC.** Allopurinol enhances the contractile response to dobutamine and exercise in dogs with pacing-induced heart failure. *Circulation* 103: 750–755, 2001.
112. **Van Remmen H, Ikeno Y, Hamilton M, Pahlavani M, Wolf N, Thorpe SR, Alderson NL, Baynes JW, Epstein CJ, Huang TT, Nelson J, Strong R, Richardson A.** Life-long reduction in MnSOD activity results in increased DNA damage and higher incidence of cancer but does not accelerate aging. *Physiol Genomics* 16: 29–37, 2003.
113. **Williams RS.** Mitochondrial gene expression in mammalian striated muscle. Evidence that variation in gene dosage is the major regulatory event. *J Biol Chem* 261: 12390–12394, 1986.
114. **Witteles RM, Tang WH, Jamali AH, Chu JW, Reaven GM, Fowler MB.** Insulin resistance in idiopathic dilated cardiomyopathy: a possible etiologic link. *J Am Coll Cardiol* 44: 78–81, 2004.
115. **Wu C, Yan L, Depre C, Dhar SK, Shen YT, Sadoshima J, Vatner SF, Vatner DE.** Cytochrome c oxidase III as a mechanism for apoptosis in heart failure following myocardial infarction. *Am J Physiol Cell Physiol* 297: C928–C934, 2009.
116. **Yamato M, Shiba T, Yoshida M, Ide T, Seri N, Kudou W, Kinugawa S, Tsutsui H.** Fatty acids increase the circulating levels of oxidative stress factors in mice with diet-induced obesity via redox changes of albumin. *FEBS J* 274: 3855–3863, 2007.
117. **Zima AV, Blatter LA.** Redox regulation of cardiac calcium channels and transporters. *Cardiovasc Res* 71: 310–321, 2006.

Circulation Journal
Official Journal of the Japanese Circulation Society
http://www.j-circ.or.jp

ORIGINAL ARTICLE
Heart Failure

Novel Strain Rate Index of Contractility Loss Caused by Mechanical Dyssynchrony

– A Predictor of Response to Cardiac Resynchronization Therapy –

Hiroyuki Iwano, MD; Satoshi Yamada, MD, PhD; Masaya Watanabe, MD; Hirofumi Mitsuyama, MD, PhD; Hisao Nishino; Shinobu Yokoyama; Sanae Kaga; Mutsumi Nishida, PhD; Hisashi Yokoshiki, MD, PhD; Hisao Onozuka, MD, PhD; Taisei Mikami, MD, PhD; Hiroyuki Tsutsui, MD, PhD

Background: Time-delay indexes are limited in predicting the response to cardiac resynchronization therapy (CRT), partly because they do not reflect the residual left ventricular (LV) contractility. We computed a novel index of LV contractility loss due to dyssynchrony (the strain rate (SR) dispersion index: SRDI) by using the speckle-tracking SR and compared the efficacy of the SRDI, time-delay indexes, and strain delay index (SDI), the previously reported index of wasted energy due to dyssynchrony, for predicting the acute response to CRT.

Methods and Results: Echocardiography was performed in 19 heart failure patients (LV ejection fraction (EF) 25±6%) before and 2 weeks after CRT. The standard deviation of time to peak velocity, or strain, was calculated as time-delay indexes. The SRDI was calculated as the average of segmental peak systolic SR minus global peak systolic SR. Longitudinal SDI (L-SDI), longitudinal SRDI (L-SRDI), and circumferential SRDI (C-SRDI) significantly correlated with the change in global longitudinal strain (Δglobal LSt), whereas the time-delay indexes did not. Although the time-delay indexes were comparable between responders (Δglobal LSt ≥0.3%) and nonresponders, the L-SDI, L-SRDI, and C-SRDI were greater in responders. The area under the receiver operating characteristic curve of the L-SRDI, L-SDI, and C-SRDI for predicting responders was 0.89, 0.81, and 0.78, respectively.

Conclusions: The SRDI correlated fairly well with an improvement in global LV systolic function after CRT. (*Circ J* 2011; **75:** 2167–2175)

Key Words: Cardiac resynchronization therapy; Echocardiography; Heart failure; Left ventricular dyssynchrony; Left ventricular systolic function

Cardiac resynchronization therapy (CRT) has been shown to improve left ventricular (LV) function and mortality in patients with advanced heart failure.[1–5] However, 30–40% of the patients who meet the standard selection criteria of widened QRS complex and low LV ejection fraction (EF) do not respond to CRT.[2,6] Thus, it has been emphasized that LV mechanical dyssynchrony should be evaluated to predict the response to CRT, which has been estimated by time-delay indexes derived from the time-delay measurement of regional wall motion using velocity data acquired with tissue Doppler imaging (TDI).[7–9] However, in the multicenter Predictors of Responders to CRT (PROSPECT) trial, the time-delay indexes assessed by TDI could not accurately predict the responses to CRT.[10] One of the reasons for these disappointing results was thought to be the high variability of the time-delay indexes.[10] In addition, because conduction disturbance, such as left bundle branch block, causes redistribution of myocardial shortening and external work, resulting a reduction in LV global systolic function,[11–13] the amount of wasted contractility related to LV dyssynchrony should be taken into account in the prediction of CRT response.[14–17]

Lim et al proposed a strain delay index (SDI), using myocardial strain assessed by the 2-dimensional speckle tracking method (2DST), to estimate the potential for incremental contractility gain after CRT.[18] This index could reflect not only the time-delay of regional wall motion but also the amount of wasted energy related to LV dyssynchrony. In

Received October 29, 2010; revised manuscript received April 13, 2011; accepted April 28, 2011; released online July 14, 2011
Time for primary review: 68 days

Department of Cardiovascular Medicine, Hokkaido University Graduate School of Medicine, Sapporo (H.I., S.Yamada, M.W., H.M., H.Y., H.T.); Division of Clinical Laboratory and Transfusion Medicine, Hokkaido University Hospital, Sapporo (H.N., S.Yokoyama, S.K., M.N.); and Faculty of Health Sciences, Hokkaido University, Sapporo (H.O., T.M.), Japan

Mailing address: Satoshi Yamada, MD, PhD, Department of Cardiovascular Medicine, Hokkaido University Graduate School of Medicine, Kita-15, Nishi-7, Kita-ku, Sapporo 060-8638, Japan. E-mail: syamada@med.hokudai.ac.jp

ISSN-1346-9843 doi:10.1253/circj.CJ-10-1099

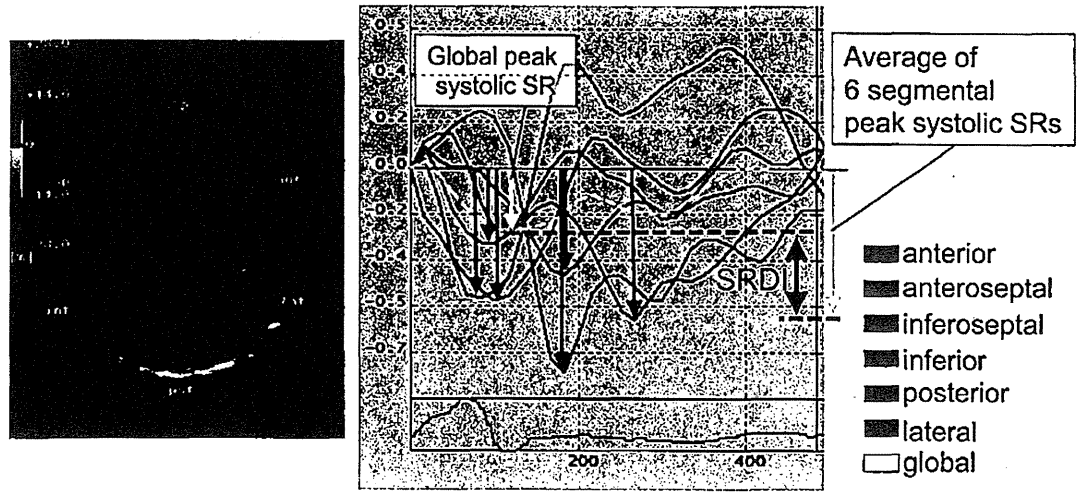

Figure 1. Demonstrable circumferential strain rate (SR) curves (**Right**) obtained from 6 segments (**Left**). The 6 colored curves indicate segmental SRs and the white, dashed curve indicates global SR. The strain rate dispersion index (SRDI) was calculated by subtracting the global peak systolic SR (white arrow) from the averaged segmental peak systolic SR (yellow arrow).

fact, they demonstrated that the SDI predicted LV reverse remodeling after CRT better than Doppler- or 2DST-derived time-delay indexes.[18] However, the myocardial strain rate (SR) may be more suitable for the evaluation of LV contractility because it is thought to be less load-dependent than strain.[19] We thus constructed an index to estimate the amount of LV contractility loss caused by dyssynchrony by using the 2DST-derived SR. The aim of the present study was to determine whether our new index, the SR dispersion index (SRDI), correlates better with the change in LV systolic function by CRT than either the time-delay indexes or the SDI.

Methods

Study Subjects and Protocol

Our study group comprised 26 consecutive patients with heart failure referred for CRT device implantation in Hokkaido University Hospital. The criteria for CRT were: (1) the presence of drug-refractory symptomatic heart failure (New York Heart Association (NYHA) functional class III or IV), (2) depressed LV systolic function defined as EF≤35%, and (3) prolonged QRS duration (≥120 ms).[20] Transthoracic echocardiography including TDI and 2DST was performed before and 2 weeks after implantation of the CRT device. The study protocol was approved by the Ethics Committee of the Hokkaido University, and all patients gave informed consent before participation in the study.

CRT Device Implantation

The LV lead of the CRT device was inserted through the coronary sinus and positioned into the lateral or posterolateral cardiac vein with the help of a venogram. The right atrial and ventricular leads were positioned conventionally, and all leads were connected to the device. A dual-chamber biventricular implantable cardioverter-defibrillator (Concerto, Medtronic or Contak Renewal 4, Guidant Corporation) was implanted in all patients, except one in whom a CRT without defibrillator was implanted.

Echocardiography

All studies were performed with a commercially available ultrasound system (Aplio SSA-770A, Toshiba Medical Systems, Tochigi, Japan) with a 2.5-MHz phased array transducer. Digital 2D and color TDI cine loops were obtained in the apical 4-, 2-, and 3-chamber, and midventricular short-axis views. Care was taken to acquire the cine loops that have close intervals of the R to R wave for analysis of 2DST and TDI in patients with atrial fibrillation. The frame rates were 44–62/s (57±8) for 2D imaging used for 2DST, and 54–69/s (58±5) for TDI. The velocity range for TDI was ±15 cm/s.

LV end-diastolic and end-systolic volumes were measured from the apical 4- and 2-chamber images using the biplane method of disks, and EF was calculated.[21] In patients with atrial fibrillation, LV volumes were measured over 5 consecutive beats, and these values were averaged. The mitral regurgitation was graded as severe when the volume measured by the proximal isovelocity surface area method was more than 60 ml.[22]

TDI Analysis

The color TDI cine loops were analyzed off-line using commercial software (TDI-Q, Toshiba Medical Systems, Tochigi, Japan). Longitudinal tissue velocities of the LV wall were measured in the basal and mid segments in 3 apical views for a total of 12 segments. Time from the onset of QRS to peak systolic velocity during the ejection phase was measured in each segment. Next, the standard deviation of time to peak systolic velocity (TDI-SD) was calculated within the 12 segments.[8] The ejection phase was defined as the period from aortic valve opening to closure as determined by LV outflow using the pulsed Doppler method.

Speckle-Tracking Strain Analysis

Myocardial strain and SR were analyzed using 2DST software (Toshiba Medical Systems, Tochigi, Japan). The LV endocardial and epicardial borders were manually traced on an end-diastolic frame for the 3 apical views and on an end-

Table 1. Baseline Characteristics of the Study Patients

	All (n=19)	Responders (n=10)	Nonresponders (n=9)	P value
Age (year)	57±12	52±12	62±10	0.067
Male, n (%)	13 (84)	7 (70)	6 (67)	0.88
NYHA class, n (%)				
III	15 (79)	8 (80)	7 (78)	0.91
IV	4 (21)	2 (20)	2 (22)	0.91
Ischemic cardiomyopathy, n (%)	4 (21)	1 (10)	3 (33)	0.21
Electrocardiographic findings				
Atrial fibrillation, n (%)	2 (11)	0 (0)	2 (22)	0.13
QRS duration (ms)	164±24	167±27	161±22	0.63
Left bundle branch block, n (%)	11 (58)	6 (60)	5 (56)	0.84
Right ventricular pacing, n (%)	4 (21)	3 (30)	1 (11)	0.31
Echocardiographic findings				
LV end-diastolic volume (ml)	226±125	196±81	260±159	0.28
LV end-systolic volume (ml)	172±111	148±63	199±147	0.33
LV ejection fraction (%)	25±6	25±4	26±8	0.65
Global longitudinal strain (%)	−4.9±1.8	−4.6±1.9	−5.1±1.9	0.56
Severe MR, n (%)	6 (32)	2 (20)	4 (44)	0.25
Medication, n (%)				
ACEI or ARB	16 (84)	8 (80)	8 (89)	0.60
β-blocker	16 (84)	9 (90)	7 (78)	0.47
Diuretic	19 (100)	10 (100)	9 (100)	
Spironolactone	11 (58)	3 (30)	8 (89)	0.009
Amiodarone	9 (47)	5 (50)	4 (44)	0.81

P values are for comparison between responders and nonresponders.
NYHA, New York Heart Association; LV, left ventricular; MR, mitral regurgitation; ACEI, angiotensin converting enzyme inhibitor; ARB, angiotensin II receptor blocker.

Table 2. Echocardiographic and Electrocardiographic Parameters at Baseline and After CRT

	Overall (n=19)		Responders (n=10)		Nonresponders (n=9)		P value
	Baseline	After CRT	Baseline	After CRT	Baseline	After CRT	
LV end-diastolic volume (ml)	226±125	212±116*	196±81	186±84	260±159	242±142	0.650
LV end-systolic volume (ml)	172±111	154±95†	148±63	130±61*	199±147	180±122	0.276
LV ejection fraction (%)	25±6	29±6‡	25±4	30±4‡	26±8	27±7	0.331
Global longitudinal strain (%)	−4.9±1.8	−5.3±1.9	−4.6±1.9	−6.0±1.8†	−5.1±1.9	−4.5±1.7*	0.555
Global longitudinal SR (s^{-1})	−0.24±0.09	−0.25±0.09	−0.24±0.10	−0.29±0.09*	−0.24±0.09	−0.22±0.73	0.996
Global circumferential SR (s^{-1})	−0.38±0.18	−0.43±0.22	−0.41±0.18	−0.52±0.25†	−0.34±0.19	−0.33±0.16	0.455
Global radial SR (s^{-1})	0.55±0.28	0.63±0.34	0.61±0.32	0.79±0.36	0.52±0.20	0.44±0.19	0.358
QRS duration (ms)	164±24	145±25†	167±27	147±24†	161±22	143±27	0.629
TDI-SD (ms)	48±10	38±13†	47±9	35±14†	48±11	41±13	0.832
LS-SD (ms)	125±51	103±30	128±53	105±32	123±51	100±30	0.819
CS-SD (ms)	91±42	75±38	80±43	61±28	102±41	89±43	0.261
RS-SD (ms)	142±54	85±47†	148±63	58±28†	135±42	132±48	0.693
L-SDI (%)	17.4±9.5	14.4±2.7	22.2±8.8	14.1±2.8*	12.2±7.6	14.7±2.7	0.017
C-SDI (%)	5.9±2.9	3.1±1.6†	6.9±3.2	2.9±1.9†	4.8±2.3	3.3±1.2	0.128
R-SDI (%)	15.7±7.8	9.2±4.7†	18.5±8.4	6.9±3.7†	12.2±6.4	12.1±4.4	0.100
L-SRDI (s^{-1})	0.19±0.09	0.17±0.05	0.25±0.08	0.16±0.05*	0.13±0.07	0.16±0.05	0.004
C-SRDI (s^{-1})	0.15±0.10	0.09±0.05†	0.19±0.10	0.10±0.05*	0.10±0.08	0.07±0.05	0.049
R-SRDI (s^{-1})	0.41±0.21	0.29±0.14	0.48±0.26	0.26±0.08*	0.32±0.10	0.34±0.19	0.130

P values are for comparison of responders and nonresponders at baseline. *P<0.05 vs. baseline, †P<0.01 vs. baseline, ‡P<0.001 vs. baseline.
CRT, cardiac resynchronization therapy; LV, left ventricular; SR, strain rate; TDI-SD, standard deviation of time to segmental peak velocities by tissue Doppler imaging; LS-SD, standard deviation of time to segmental peak longitudinal strain; CS-SD, standard deviation of time to segmental peak circumferential strain; RS-SD, standard deviation of time to segmental peak radial strain; L-SDI, longitudinal strain delay index; C-SDI, circumferential strain delay index; R-SDI, radial strain delay index; L-SRDI, longitudinal strain rate dispersion index; C-SRDI, circumferential strain rate dispersion index; R-SRDI, radial strain rate dispersion index.

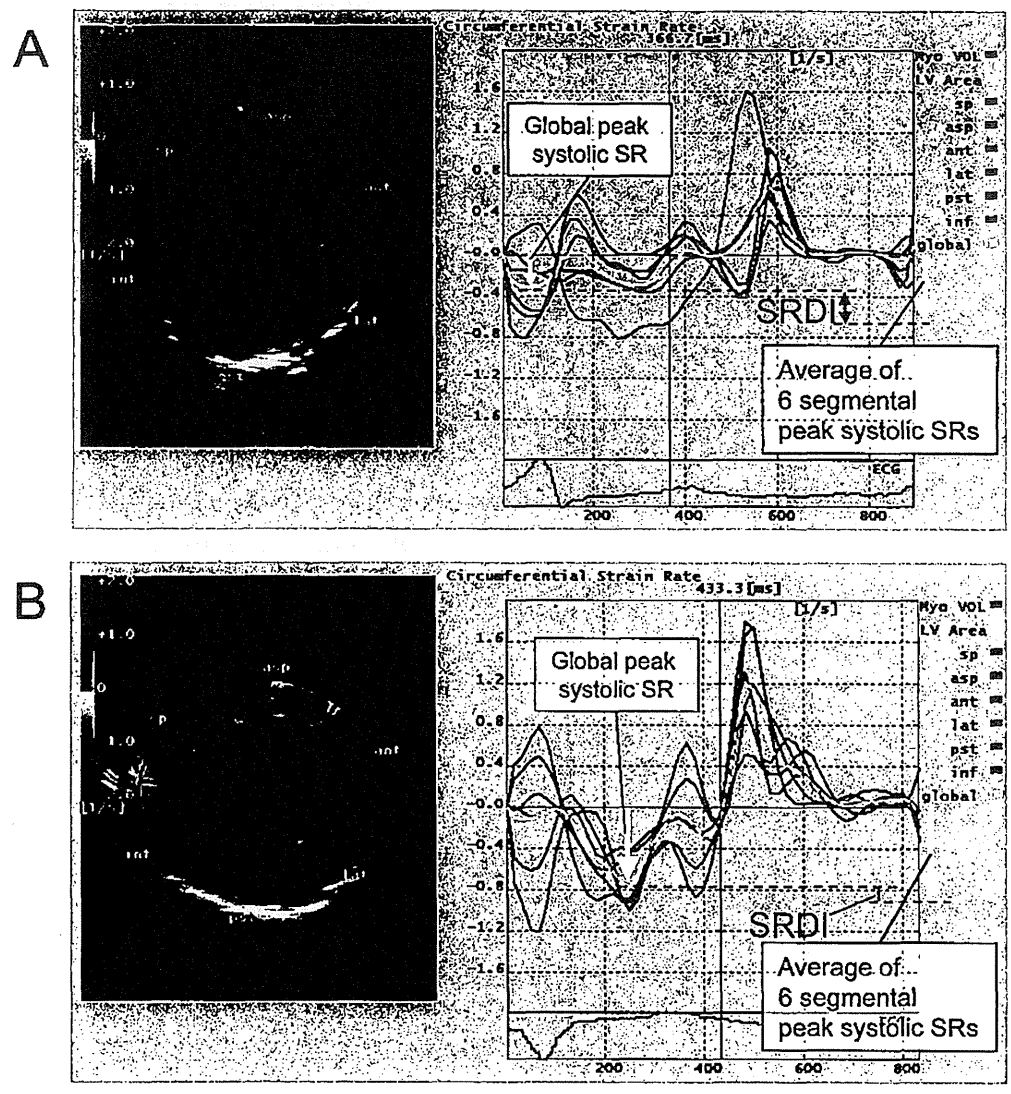

Figure 2. Time–circumferential strain rate curve obtained from a responder before (**A**) and 2 weeks after CRT (**B**). Note that the value of global peak systolic strain rate (white arrow in **B**) increased by CRT up to the level of average of 6 segmental peak systolic SRs at baseline (yellow arrow in **A**). SR, strain rate; SRDI, strain rate dispersion index.

systolic frame for the midventricular short-axis view. LV wall was divided into 6 segments within each view, and the time-strain and time–SR curves for each segment were extracted by automated tracking of the endocardial border for the longitudinal and circumferential indexes and that of both the endocardial and epicardial borders for the radial indexes. Longitudinal strain/SR curves were obtained from 3 apical views, and circumferential and radial strain/SR from the short-axis view. The standard deviation of time from the onset of QRS to segmental peak strain was calculated for the longitudinal, circumferential, and radial strains (LS-SD, CS-SD, and RS-SD, respectively).

The time-global strain curve was also extracted as reported by Lim et al, determining end-systole as the time point of peak global strain.[18] Briefly, to correct the differences of the R to R intervals among the apical images, strain values of all segments were averaged at every 2.5% of the R to R interval for the calculation of global longitudinal strain. Global circumferential and radial strains were obtained by averaging 6 segmental strains at each frame in the short-axis view. Peak strain (ε_{peak}) and strain at end-systole (ε_{ES}) were measured in each segment. Next, the longitudinal SDI (L-SDI) was measured as the sum of ($\varepsilon_{peak}-\varepsilon_{ES}$) from the 16 segments in the 3 apical views. The circumferential SDI (C-SDI) and radial SDI (R-SDI) were calculated from 6 segments in the short-axis view. In the segments that showed the strain in the stretching direction or biphasic strain with the absolute value of the stretching strain greater than the shortening strain, ($\varepsilon_{peak}-\varepsilon_{ES}$) were counted as zero.[18]

The SRDI was calculated as a new index of global LV

contractility loss caused by dyssynchrony. Peak systolic SRs were measured in all segments within each view. We also extracted the time–global SR curve by averaging all segmental SRs at every 2% of the R to R interval and measured global peak systolic SR. The SRDI was then calculated as the average of the segmental peak systolic SRs minus global peak systolic SR (**Figure 1**). The longitudinal SRDI (L-SRDI) was derived from the 3 apical views, and the circumferential SRDI (C-SRDI) and radial SRDI (R-SRDI) were derived from the short-axis view.

The accuracy of speckle tracking for each myocardial segment was visually judged by 2 independent observers. Patients who had 2 or more segments judged as having inadequate tracking quality in at least one view were excluded.

Estimation of LV Systolic Function

LV systolic function was estimated by global longitudinal strain and EF before and 2 weeks after CRT. Response to CRT were defined as an improvement of ≥0.3% in global longitudinal strain at follow-up.

Statistical Analysis

Continuous variables are expressed as mean±SD and compared with the 2-tailed Student's t-test for paired and unpaired data. Proportions were compared using chi-square analysis. Linear regression analysis was carried out for the detection of correlation between 2 continuous variables. Receiver-operating characteristic (ROC) curves were determined to evaluate the diagnostic performance of the time-delay indexes and indexes of LV contractility loss to detect responders to CRT. For all tests, $P<0.05$ was considered significant.

Results

Patients' Baseline Characteristics

Of the 26 patients, 7 were excluded because of inadequate tracking quality of 2DST. Thus, the final study group consisted of 19 patients, whose baseline characteristics are summarized in **Table 1**. All patients had heart failure symptoms (NYHA class III or IV) with severe LV dysfunction and wide QRS duration; 15 patients had left bundle branch block (58%) or right ventricular pacing rhythm (21%) and the other causes of prolonged QRS duration were intraventricular conduction disturbance in 3 patients and right bundle branch block in 1 patient. Etiology was ischemic for 21% of all patients. Medications were optimal for heart failure, including angiotensin-converting enzyme inhibitors or angiotensin II receptor blockers, β-blockers, diuretics, and spironolactone.

Acute Responses to CRT

A CRT device was successfully implanted in all patients without any complications. None of the patients died or underwent heart transplantation during the follow-up. Two weeks after the implantation of the CRT device, NYHA functional class was significantly reduced from 3.2±0.4 to 2.8±0.4 ($P<0.05$). The QRS duration decreased. EF significantly increased and global longitudinal strain tended to increase after CRT, but did not reach statistical significance (**Table 2**). Global longitudinal, circumferential, and radial SRs did not change after CRT in the overall patient group. There was a significant correlation between EF and global longitudinal strain ($R=-0.57$, $P<0.001$).

The time-delay indexes, such as TDI-SD and RS-SD, and indexes of LV contractility loss, including the C-SDI, R-SDI, and C-SRDI, significantly decreased from baseline values after CRT, whereas the LS-SD, CS-SD, L-SDI, L-SRDI, and R-SRDI did not change (**Table 2**).

Table 3. Correlation Between Echocardiographic Parameters and the Change in LV Systolic Function by CRT

	Δglobal longitudinal strain		ΔEF	
	R	P value	R	P value
QRS duration	−0.31	0.204	0.41	0.09
TDI-SD	−0.09	0.712	0.05	0.83
LS-SD	−0.40	0.090	0.27	0.26
CS-SD	−0.02	0.941	−0.09	0.73
RS-SD	−0.31	0.198	0.14	0.56
L-SDI	−0.59	0.008	0.64	0.003
C-SDI	−0.30	0.220	0.29	0.23
R-SDI	−0.26	0.279	0.23	0.34
L-SRDI	−0.69	0.001	0.76	<0.001
C-SRDI	−0.47	0.045	0.34	0.15
R-SRDI	−0.36	0.13	0.28	0.24

Abbreviations see in Tables 1,2.

Acute Responses in Responders vs. Nonresponders

Among the 19 patients, there were 10 acute responders (53%) defined as an increase in global longitudinal strain after CRT (Δglobal LSt) ≥0.3%. The remaining 9 patients (47%) were classified as nonresponders. Responders showed a significant increase in EF and a slightly but significant decrease in LV end-systolic volume (**Table 2**). In contrast, nonresponders showed no changes in either of these parameters. Moreover, responders showed significantly improved global longitudinal strain, global longitudinal SR, and global circumferential SR whereas nonresponders did not. Global radial SR tended to increase in responders, but did not reach statistical significance (**Table 2**). Among the responders, QRS duration decreased (**Table 2**). RS-SD significantly decreased with CRT in the responders but not LS-SD and CS-SD (**Table 2**). The L-SDI, C-SDI, R-SDI, L-SRDI, C-SRDI, and R-SRDI all decreased with CRT in the responders (**Table 2, Figure 2**). In contrast, none of these parameters changed in the nonresponders (**Table 2**).

Prediction of Response to CRT

Baseline clinical and echocardiographic parameters were comparable between responders and nonresponders, except for spironolactone use (**Table 1**). The L-SDI, L-SRDI and C-SRDI at baseline were significantly higher in responders than in nonresponders (**Table 2**).

Linear regression analyses showed that neither QRS duration nor the TDI-SD at baseline correlated with Δglobal LSt (**Table 3**). The LS-SD, CS-SD, RS-SD, C-SDI, R-SDI, and R-SRDI did not correlate with Δglobal LSt (**Table 3, Figure 3**). In contrast, the L-SDI, L-SRDI and C-SRDI significantly correlated with Δglobal LSt (**Table 3, Figure 3**). Similar trend was observed when LV systolic function was estimated by EF (**Table 3**).

ROC analyses for predicting the responders showed that, among these parameters, the L-SRDI had the largest area under the ROC curve. The L-SDI, L-SRDI, and C-SRDI could significantly discriminate between responders and nonresponders (**Table 4**).

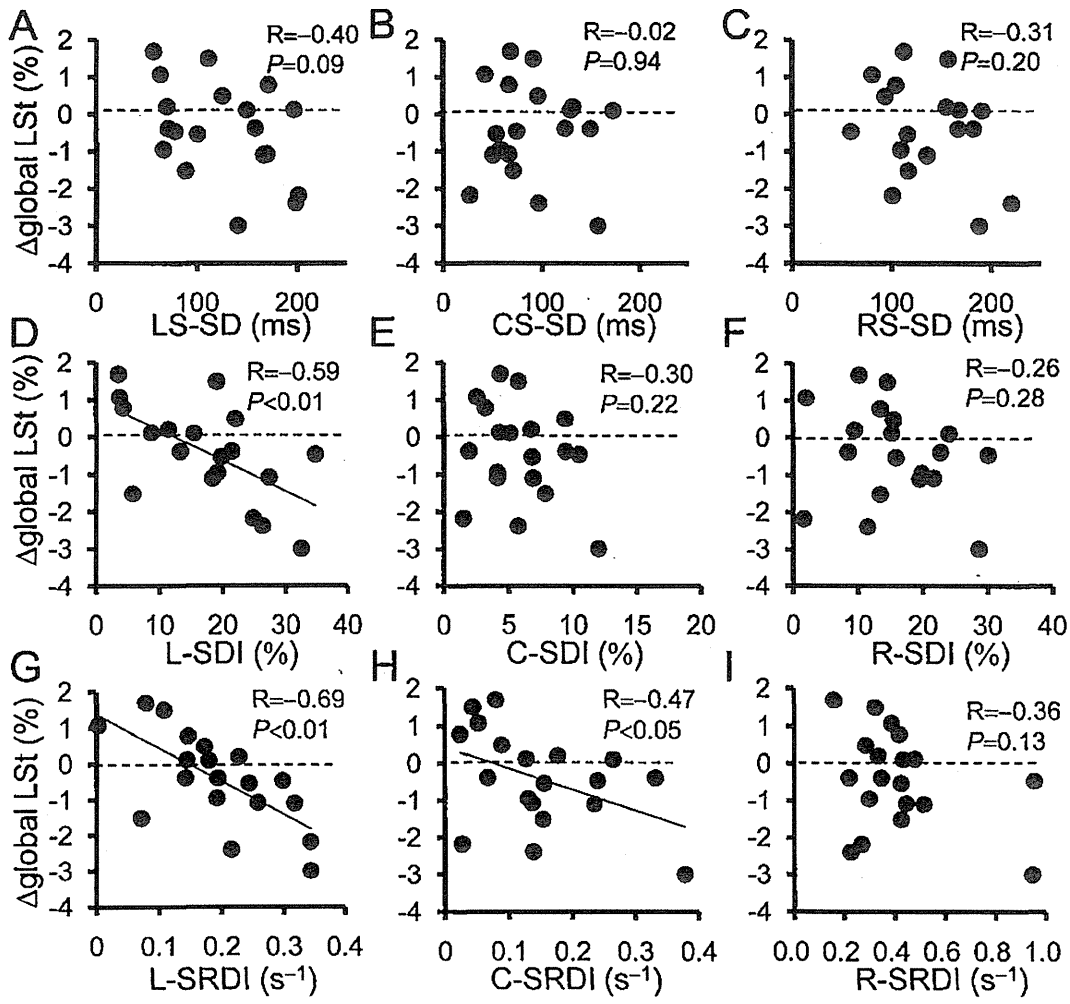

Figure 3. Correlations between Δglobal LSt and LS-SD (**A**), CS-SD (**B**), RS-SD (**C**), L-SDI (**D**), C-SDI (**E**), R-SDI (**F**), L-SRDI (**G**), C-SRDI (**H**), and R-SRDI (**I**). Δglobal LSt, changes in global longitudinal strain before and after CRT. LS-SD, standard deviation of time to peak longitudinal strain; CS-SD, standard deviation of time to peak circumferential strain; RS-SD, standard deviation of time to peak radial strain; L-SDI, longitudinal strain delay index; C-SDI, circumferential strain delay index; R-SDI, radial strain delay index; L-SRDI, longitudinal strain rate dispersion index, C-SRDI, circumferential strain rate dispersion index; R-SRDI, radial strain rate dispersion index.

Table 4. AUC for Predicting Responders to CRT

	AUC	95% CI	P value
TDI-SD	0.49	0.21–0.77	0.94
LS-SD	0.57	0.30–0.84	0.62
CS-SD	0.34	0.09–0.60	0.25
RS-SD	0.54	0.28–0.81	0.74
L-SDI	0.81	0.62–1.00	0.02
C-SDI	0.70	0.50–0.97	0.14
R-SDI	0.73	0.49–0.98	0.09
L-SRDI	0.89	0.70–1.00	0.006
C-SRDI	0.78	0.55–1.00	0.04
R-SRDI	0.68	0.43–0.92	0.19

P values are for AUCs vs. the null hypothesis of a true area of 0.5. AUC, area under the receiver-operating curve; CI, confidence interval. Other abbreviations see in Table 2.

Reproducibility

Intra- and interobserver variabilities of EF were both 7% in our laboratory. Reproducibility of strain and SR measurements were assessed in 10 randomly selected patients. Analyses of global longitudinal strain, LS-SD, CS-SD, RS-SD, L-SDI, C-SDI, R-SDI, L-SRDI, C-SRDI, and R-SRDI were performed by 2 independent observers using the same 2D cine loop and the same cardiac cycle. A single blinded observer repeated the analyses after an interval of 2 weeks. The respective intra- and interobserver variabilities were 0.5% (9%) and 0.5% (10%) for global longitudinal strain, 12 ms (10%) and 20 ms (16%) for LS-SD, 17 ms (18%) and 19 ms (19%) for CS-SD, 26 ms (20%) and 31 ms (24%) for RS-SD, 1.9% (12%) and 3.0% (17%) for L-SDI, 0.9% (16%) and 0.9% (17%) for C-SDI, 2.9% (19%) and 3.9% (25%) for R-SDI, 0.02 s^{-1} (10%) and 0.03 s^{-1} (17%) for L-SRDI, 0.02 s^{-1}

(13%) and 0.02 s^{-1} (15%) for C-SRDI, and 0.07 s^{-1} (18%) and 0.09 s^{-1} (22%) for R-SRDI.

Discussion

This is the first study to demonstrate that a novel index of LV contractility loss because of dyssynchrony, the SRDI, could predict acute responders to CRT. Furthermore, the SRDI correlated well with the improvement in LV systolic function.

CRT has been shown to improve LV function and survival in NYHA III–IV patients with severe LV dysfunction and a wide QRS.[1–5] However, more than 30% of patients selected on the basis of QRS duration do not respond to CRT,[2,6] suggesting that mechanical rather than electrical dyssynchrony can better predict the response to CRT. Measurement of regional peak-systolic velocities with TDI has been shown to be highly predictive for the response to CRT and prognosis.[7–9] However, limitations of the time-delay indexes measured by TDI to assess LV mechanical dyssynchrony for the prediction of response to CRT have been reported.[10,23] The limited accuracy of the TDI parameters to predict the response to CRT might have several reasons. First, the accuracy of measurement of regional myocardial velocities by TDI is limited by ultrasound angle dependency and tethering effects, which are especially prominent in the dilated LV commonly seen in patients with severe heart failure who require CRT.[24,25] Second and more importantly, the time-delay indexes do not take regional myocardial contractility into account. In the presence of a conduction disturbance, especially in left bundle branch block or right ventricular pacing, asynchronous electrical activation causes redistribution of myocardial shortening and external work, which is associated with a reduction in LV global systolic function.[11–13] CRT improves the heterogeneity of myocardial shortening by activation of the latest activated site, resulting in augmentation of global LV contractility.[26] Therefore, dyscoordination of contraction can more directly associate with the improvement of LV systolic function by CRT than the dispersion of the timing of regional contraction. In fact, the present study demonstrated that the time-delay indexes derived from TDI and 2DST could not predict the changes in LV systolic function (Tables 3,4).

The indexes of dyscoordination, which measure the amount of both myocardial stretch and shortening during systole, were recently reported to better correlate with the immediate[15] and chronic responses to CRT[14,16,17] than the time-delay indexes. The SDI, an index of wasted energy caused by dyssynchrony, has been also reported as a strong predictor of the response to CRT.[18] This index can account for the difference between ε_{peak} and ε_{ES}, which represents wasted energy caused by dyssynchrony per segment and sums these values in all LV segments. The SDI can be regarded as a dyscoordination index, but is somewhat different because it does not measure the amount of stretch. Therefore, we consider that our new index, the SRDI, is a logical extension of SDI. The concept of the SRDI is based on the idea that the wasted contractility from mechanical dyssynchrony can be the acute gain of contractility expected to be obtained by CRT. The average of the segmental peak systolic SR was estimated as global LV systolic function when the contraction is synchronized and global peak systolic SR was measured as the actual global LV systolic function in the presence of mechanical dyssynchrony. Therefore, the SRDI, the difference between the estimated and actual global LV systolic function, can estimate the increase of global LV systolic function by the correction of dyssynchrony. Indeed, the present results demonstrated that the SRDI correlated better than the time-delay indexes with the changes in LV systolic function by CRT.

The present results support previous findings that indexes of LV systolic function wasted by mechanical dyssynchrony correlate better with the CRT response than the time-delay indexes.[14–18] Our study, as well as that by Lim et al, demonstrated that both the SDI and SRDI correlated with the changes in LV systolic function after CRT. We thus consider that our index, the SRDI, is suitable for predicting the acute response to CRT for several reasons. First, although myocardial strain substantially depends on the afterload, the myocardial SR is less load-dependent.[19] Therefore, SR can more accurately reflect regional systolic function than strain. Second, the segment that shows biphasic strain with myocardial stretching, (ε_{peak}–ε_{ES}) is estimated as zero for the calculation of SDI, which is acceptable in a segment with predominantly scarred myocardium. On the contrary, in the segment with viable myocardium remaining, the SDI may underestimate regional systolic function. In contrast, the SRDI can detect the decreased contractility of residual viable myocardium by measuring segmental peak systolic SR. Third, for the calculation of the SDI, the strain values need to be measured at 2 time points for each segment, whereas the SRDI can be calculated by measuring only the peak SR for each segment and the peak SR on the global SR curve. In addition, the 2DST-software can automatically measure the peak SR on a time–SR curve. Hence, the SRDI is a simpler than the SDI and can be used more easily in routine clinical practice.

It is generally considered that the reproducibility of the SR is substantially lower than that of strain when derived from 2DST. In the present study, however, the reproducibilities of the SDI and SRDI were similar. The calculation of the SDI needs 2 time points to be measured for each segmental strain curve, whereas the SRDI can be calculated by measuring peak SR alone for each segment. This difference in the number of measurement points could be a reason why the reproducibility of the SRDI was not worse than that of the SDI. In addition, the image quality was relatively good in our study population, resulting in less noisy SR curves being obtained in most of the patients.

Study Limitations

First, the results were obtained from a relatively small number of patients in a single center. Therefore, we have to acknowledge that this study is preliminary and further study with a larger number of patients is necessary to confirm the efficacy of the SRDI. Second, the SRDI cannot be applied to the patients for whom optimal echocardiographic images are not available. We excluded 7 of the original 26 patients (27%) because of inadequate image quality, whichis is similar to the 30% excluded by Lim et al.[18] Third, we have to acknowledge that the follow-up period was short. We analyzed only the immediate changes in LV systolic function by CRT whereas the response to CRT is usually a combination of both immediate changes in systolic function and short-term reduction of LV volumes.[27] Thus, it must be determined whether the SRDI is effective in predicting the longer term beneficial response to CRT. In addition, we evaluated LV systolic function by global longitudinal strain, because it is generally considered to be a more sensitive marker of systolic function than EF. Even though the cut-off values of global longitudinal strain were somewhat arbitrary, it was significantly correlated with EF in our study patients.

Moreover, the parallel behavior between global strain and EF has been confirmed by the previous study by Brown et al.[28] Fourth, although the frame rates of 2DST were comparable to those used in a previous report of the 2DST-derived SR,[29] those of the TDI were considerably low, which could reduce the accuracy of the TDI-SD. Fifth, contrary to previously reported results,[16,30,31] none of the radial indexes correlated with the changes in LV systolic function after CRT in the present study. The automated tracking of both the endo- and epicardial borders obtained from the dilated LV, in which adequate images including the entire epicardium were difficult to obtain, might deteriorate the reproducibility of radial indexes. We consider this lead to the radial indexes being ineffective in predicting the response to CRT. Sixth, because the dispersion of the timing of the peak SRs was not analyzed, we could not demonstrate a uniform comparison of timing vs. amplitude parameters for both strain and SR in the present study. Seventh, the L-SDI and L-SRDI strongly correlated with the changes in LV systolic function after CRT in the present study, whereas the C-SDI and C-SRDI had a weak correlation. Lim et al also reported that longitudinal strain better reflected regional or global wall motion than circumferential or radial strain.[18] On the other hand, studies using magnetic resonance imaging reported the utility of circumferential strain for the evaluation of mechanical dyssynchrony.[32,33] Therefore, it remains to be determined which direction of strain/SR can better predict functional improvement after CRT and further investigations are needed to clarify this issue.

Conclusions

SRDI, a novel index of LV contractility loss because of mechanical dyssynchrony, correlated fairly well with an improvement of global LV systolic function after CRT. This new index is expected to be predictive of the long-term beneficial effects of CRT.

References

1. St John Sutton MG, Plappert T, Abraham WT, Smith AL, DeLurgio DB, Leon AR, et al. Effect of cardiac resynchronization therapy on left ventricular size and function in chronic heart failure. *Circulation* 2003; **107**: 1985–1990.
2. Cleland JG, Daubert JC, Erdmann E, Freemantle N, Gras D, Kappenberger L, et al. The effect of cardiac resynchronization on morbidity and mortality in heart failure. *N Engl J Med* 2005; **352**: 1539–1549.
3. Abraham WT, Fisher WG, Smith AL, Delurgio DB, Leon AR, Loh E, et al. Cardiac resynchronization in chronic heart failure. *N Engl J Med* 2002; **346**: 1845–1853.
4. Hiramitsu S, Miyagishima K, Kimura H, Mori K, Shiino K, Yamada A, et al. Management of severe heart failure. *Circ J* 2009; **73**: A-36–A-41.
5. Ferrari R, Ceconi C, Campo G, Cangiano E, Cavazza C, Secchiero P, et al. Mechanisms of remodeling: A question of life (stem cell production) and death (myocyte apoptosis). *Circ J* 2009; **73**: 1973–1982.
6. Bleeker GB, Bax JJ, Fung JW, van der Wall EE, Zhang Q, Schalij MJ, et al. Clinical versus echocardiographic parameters to assess response to cardiac resynchronization therapy. *Am J Cardiol* 2006; **97**: 260–263.
7. Bax JJ, Bleeker GB, Marwick TH, Molhoek SG, Boersma E, Steendijk P, et al. Left ventricular dyssynchrony predicts response and prognosis after cardiac resynchronization therapy. *J Am Coll Cardiol* 2004; **44**: 1834–1840.
8. Yu CM, Chau E, Sanderson JE, Fan K, Tang MO, Fung WH, et al. Tissue Doppler echocardiographic evidence of reverse remodeling and improved synchronicity by simultaneously delaying regional contraction after biventricular pacing therapy in heart failure. *Circulation* 2002; **105**: 438–445.
9. Gorcsan J 3rd, Kanzaki H, Bazaz R, Dohi K, Schwartzman D. Usefulness of echocardiographic tissue synchronization imaging to predict acute response to cardiac resynchronization therapy. *Am J Cardiol* 2004; **93**: 1178–1181.
10. Chung ES, Leon AR, Tavazzi L, Sun JP, Nihoyannopoulos P, Merlino J, et al. Results of the Predictors of Response to CRT (PROSPECT) trial. *Circulation* 2008; **117**: 2608–2616.
11. Prinzen FW, Hunter WC, Wyman BT, McVeigh ER. Mapping of regional myocardial strain and work during ventricular pacing: Experimental study using magnetic resonance imaging tagging. *J Am Coll Cardiol* 1999; **33**: 1735–1742.
12. Nelson GS, Curry CW, Wyman BT, Kramer A, Declerck J, Talbot M, et al. Predictors of systolic augmentation from left ventricular preexcitation in patients with dilated cardiomyopathy and intraventricular conduction delay. *Circulation* 2000; **101**: 2703–2709.
13. Mills RW, Cornelussen RN, Mulligan LJ, Strik M, Rademakers LM, Skadsberg ND, et al. Left ventricular septal and left ventricular apical pacing chronically maintain cardiac contractile coordination, pump function and efficiency. *Circ Arrhythm Electrophysiol* 2009; **2**: 571–579.
14. Kirn B, Jansen A, Bracke F, van Gelder B, Arts T, Prinzen FW. Mechanical discoordination rather than dyssynchrony predicts reverse remodeling upon cardiac resynchronization. *Am J Physiol Heart Circ Physiol* 2008; **295**: H640–H646.
15. De Boeck BW, Kirn B, Teske AJ, Hummeling RW, Doevendans PA, Cramer MJ, et al. Three-dimensional mapping of mechanical activation patterns, contractile dyssynchrony and dyscoordination by two-dimensional strain echocardiography: Rationale and design of a novel software toolbox. *Cardiovasc Ultrasound* 2008; **6**: 22.
16. Wang CL, Wu CT, Yeh YH, Wu LS, Chang CJ, Ho WJ, et al. Recoordination rather than resynchronization predicts reverse remodeling after cardiac resynchronization therapy. *J Am Soc Echocardiogr* 2010; **23**: 611–620.
17. De Boeck BW, Teske AJ, Meine M, Leenders GE, Cramer MJ, Prinzen FW, et al. Septal rebound stretch reflects the functional substrate to cardiac resynchronization therapy and predicts volumetric and neurohormonal response. *Eur J Heart Fail* 2009; **11**: 863–871.
18. Lim P, Buakhamsri A, Popovic ZB, Greenberg NL, Patel D, Thomas JD, et al. Longitudinal strain delay index by speckle tracking imaging: A new marker of response to cardiac resynchronization therapy. *Circulation* 2008; **118**: 1130–1137.
19. Marwick TH. Measurement of strain and strain rate by echocardiography: Ready for prime time? *J Am Coll Cardiol* 2006; **47**: 1313–1327.
20. Hunt SA, Abraham WT, Chin MH, Feldman AM, Francis GS, Ganiats TG, et al. ACC/AHA 2005 Guideline Update for the Diagnosis and Management of Chronic Heart Failure in the Adult: A report of the American College of Cardiology/American Heart Association Task Force on Practice Guidelines (Writing Committee to Update the 2001 Guidelines for the Evaluation and Management of Heart Failure): Developed in collaboration with the American College of Chest Physicians and the International Society for Heart and Lung Transplantation: Endorsed by the Heart Rhythm Society. *Circulation* 2005; **112**: e154–e235.
21. Lang RM, Bierig M, Devereux RB, Flachskampf FA, Foster E, Pellikka PA, et al. Recommendations for chamber quantification: A report from the American Society of Echocardiography's Guidelines and Standards Committee and the Chamber Quantification Writing Group, developed in conjunction with the European Association of Echocardiography, a branch of the European Society of Cardiology. *J Am Soc Echocardiogr* 2005; **18**: 1440–1463.
22. Bonow RO, Carabello BA, Kanu C, de Leon AC Jr, Faxon DP, Freed MD, et al. ACC/AHA 2006 guidelines for the management of patients with valvular heart disease: A report of the American College of Cardiology/American Heart Association Task Force on Practice Guidelines (writing committee to revise the 1998 Guidelines for the Management of Patients With Valvular Heart Disease): Developed in collaboration with the Society of Cardiovascular Anesthesiologists: Endorsed by the Society for Cardiovascular Angiography and Interventions and the Society of Thoracic Surgeons. *Circulation* 2006; **114**: e84–e231.
23. Beshai JF, Grimm RA, Naguch SF, Baker JH 2nd, Beau SL, Greenberg SM, et al. Cardiac-resynchronization therapy in heart failure with narrow QRS complexes. *N Engl J Med* 2007; **357**: 2461–2471.
24. Suffoletto MS, Dohi K, Cannesson M, Saba S, Gorcsan J 3rd. Novel speckle-tracking radial strain from routine black-and-white echocardiographic images to quantify dyssynchrony and predict response to cardiac resynchronization therapy. *Circulation* 2006; **113**: 960–968.

25. Seo Y, Ishizu T, Sakamaki F, Yamamoto M, Machino T, Yamasaki H, et al. Mechanical dyssynchrony assessed by speckle tracking imaging as a reliable predictor of acute and chronic response to cardiac resynchronization therapy. *J Am Soc Echocardiogr* 2009; **22:** 839–846.
26. Klimusina J, De Boeck BW, Leenders GE, Faletra FF, Prinzen F, Averaimo M, et al. Redistribution of left ventricular strain by cardiac resynchronization therapy in heart failure patients. *Eur J Heart Fail* 2011; **13:** 186–194.
27. Shimizu A. Cardiac resynchronization therapy with and without implantable cardioverter-defibrillator. *Circ J* 2009; **73:** A-29–A-35.
28. Brown J, Jenkins C, Marwick TH. Use of myocardial strain to assess global left ventricular function: A comparison with cardiac magnetic resonance and 3-dimensional echocardiography. *Am Heart J* 2009; **157:** 102 e101–e105.
29. Dokainish H, Sengupta R, Pillai M, Bobek J, Lakkis N. Usefulness of new diastolic strain and strain rate indexes for the estimation of left ventricular filling pressure. *Am J Cardiol* 2008; **101:** 1504–1509.
30. Delgado V, Ypenburg C, van Bommel RJ, Tops LF, Mollema SA, Marsan NA, et al. Assessment of left ventricular dyssynchrony by speckle tracking strain imaging comparison between longitudinal, circumferential, and radial strain in cardiac resynchronization therapy. *J Am Coll Cardiol* 2008; **51:** 1944–1952.
31. Tanaka H, Nesser HJ, Buck T, Oyenuga O, Janosi RA, Winter S, et al. Dyssynchrony by speckle-tracking echocardiography and response to cardiac resynchronization therapy: Results of the Speckle Tracking and Resynchronization (STAR) study. *Eur Heart J* 2010; **31:** 1690–1700.
32. Zwanenburg JJ, Gotte MJ, Marcus JT, Kuijer JP, Knaapen P, Heethaar RM, et al. Propagation of onset and peak time of myocardial shortening in time of myocardial shortening in ischemic versus nonischemic cardiomyopathy: Assessment by magnetic resonance imaging myocardial tagging. *J Am Coll Cardiol* 2005; **46:** 2215–2222.
33. Helm RH, Leclercq C, Faris OP, Ozturk C, McVeigh E, Lardo AC, et al. Cardiac dyssynchrony analysis using circumferential versus longitudinal strain: Implications for assessing cardiac resynchronization. *Circulation* 2005; **111:** 2760–2767.

EUROPEAN SOCIETY OF CARDIOLOGY®

European Journal of Echocardiography (2011) **12**, 917–923
doi:10.1093/ejechocard/jer154

Early diastolic mitral annular velocity at the interventricular septal annulus correctly reflects left ventricular longitudinal myocardial relaxation

Kazunori Okada[1], Taisei Mikami[2]*, Sanae Kaga[3], Hisao Onozuka[2], Mamiko Inoue[3], Shinobu Yokoyama[3], Hisao Nishino[3], Mutsumi Nishida[3], Kazuhiko Matsuno[3], Hiroyuki Iwano[4], Satoshi Yamada[4], and Hiroyuki Tsutsui[4]

[1]Division of Health Sciences, Hokkaido University Graduate School of Health Sciences, Kita-12, Nishi-5, Kita-ku, Sapporo 060-0812, Japan; [2]Faculty of Health Sciences, Hokkaido University, Kita-12, Nishi-5, Kita-ku, Sapporo 060-0812, Japan; [3]Division of Laboratory and Transfusion Medicine, Hokkaido University Hospital, Kita-14, Nishi-5, Kita-ku, Sapporo 060-8648, Japan; and [4]Department of Cardiovascular Medicine, Hokkaido University Graduate School of Medicine, Kita-15, Nishi-7, Kita-ku, Sapporo 060-8638, Japan

Received 23 May 2011; accepted after revision 2 August 2011; online publish-ahead-of-print 9 September 2011

Aims Early diastolic mitral annular velocity (e′) obtained by tissue Doppler imaging (TDI) is widely used to evaluate left ventricular (LV) diastolic function based on the assumption that it reflects myocardial relaxation in the long-axis direction. In this study, we aimed to determine whether or not e′ truly reflects early diastolic longitudinal myocardial relaxation, and which is the most useful for evaluating LV diastolic function among e′ measured at the interventricular-septal annulus (IS-e′), that measured at the lateral annulus (LW-e′) or their mean value (*M*-e′).

Methods and results IS-e′, LW-e′, and *M*-e′ were measured using colour TDI in 15 patients with hypertrophic cardiomyopathy, 13 patients with hypertension, and 19 control subjects. Using two-dimensional speckle-tracking imaging, early diastolic myocardial strain rates (SR_E) were measured for the IS (IS-SR_E), LW (LW-SR_E), and entire LV myocardium (G-SR_E). IS-e′ was excellently correlated with IS-SR_E ($r = 0.90$, $P < 0.001$); the correlation was better than that between LW-e′ and LW-SR_E ($r = 0.75$, $P < 0.001$). IS-e′ and *M*-e′ were well correlated with G-SR_E ($r = 0.88$, $P < 0.001$ and $r = 0.86$, $P < 0.001$, respectively) and with LV early diastolic flow propagation velocity (FPV) ($r = 0.77$, $P < 0.001$ and $r = 0.78$, $P < 0.001$, respectively). The correlations of LW-e′ to G-SR_E ($r = 0.80$, $P < 0.001$) and FPV ($r = 0.75$, $P < 0.001$) did not reach this level.

Conclusion IS-e′ well reflected LV longitudinal myocardial relaxation and LV diastolic function, and was found to be more useful in evaluating LV diastolic function than LW-e′.

Keywords Tissue Doppler imaging • Early diastolic mitral annular velocity • Two-dimensional speckle-tracking imaging • Left ventricular longitudinal myocardial relaxation

Introduction

Early diastolic mitral annular velocity (e′) derived from tissue Doppler imaging (TDI) is widely used to evaluate left ventricular (LV) diastolic function based on the assumption that it reflects the myocardial relaxation in the long-axis direction.[1–4] It can be performed easily with excellent reproducibility,[1–6] and many investigators have reported the usefulness of the ratio of early diastolic transmitral flow velocity to e′ (*E*/e′) in estimating LV filling pressure.[1,5,7,8] In this way, the value of e′ measurement has been established through many clinical and physiological studies, but it remains still unclear whether or not the mitral annular velocity truly reflects the LV longitudinal myocardial relaxation. In addition, the measurement of e′ has been performed at the interventricular septal annulus (IS-e′)[2,5,7] and/or lateral annulus (LW-e′)[1,9] in the apical four-chamber view; their mean value (*M*-e′)[8,10] has also been used. However, it is not clear which of IS-e′, LW-e′, or *M*-e′ is the best to evaluate LV diastolic function.

* Corresponding author. Tel: +81 11 706 3403; fax: +81 11 706 4916, Email: mikami@hs.hokudai.ac.jp

Two-dimensional speckle-tracking imaging (2DSTI) is a recently developed echocardiographic technique that automatically tracks myocardial motion throughout the entire cardiac cycle on the basis of pattern-matching techniques and provides myocardial strain and strain rate.[11–13] This technique can provide an accurate evaluation of myocardial longitudinal contraction and relaxation without any angle dependency and the effect of apical translation, both of which are critical limitations of TDI. In this study, we aimed to determine whether the mitral annular velocity truly reflects the LV longitudinal myocardial relaxation and which e′ measurement, IS-e′, LW-e′, or *M*-e′, is the most useful for evaluating LV diastolic function.

Methods

Subjects

The study subjects consisted of 15 patients with hypertrophic cardiomyopathy (HCM) (11 men and 4 women, 54.3 ± 14.5 years), 13 age-matched patients with hypertension (HT) (7 men and 6 women, 52.2 ± 12.5 years), and 19 age-matched normal control subjects (11 men and 8 women, 52.6 ± 9.2 years) in whom good quality of echocardiographic images could be obtained. HCM was defined as LV hypertrophy not explained by any cardiac or systemic abnormalities and with an interventricular septal (IS) thickness/posterior wall thickness ratio in end-diastole of more than 1.3 by two-dimensional echocardiography. HT was defined as a repeatedly elevated blood pressure (>140 mmHg at systole or 90 mmHg at diastole) or having antihypertensive medications with a history of HT. We excluded patients with obvious systolic dysfunction whose echocardiographic LV ejection fraction was <55%, apparent pulmonary HT, or cardiac rhythm disturbances such as atrial fibrillation or artificial pacing. Patients with congestive heart failure, diabetes mellitus, coronary heart disease with apparent LV asynergy, congenital anomaly, valvular heart disease, or other systemic diseases that cause LV hypertrophy were also excluded. Furthermore, we excluded subjects in whom an ultrasound beam could not be inserted correctly from the apex in the apical four-chamber view.

Medications for patients with HT were β-blocker in 1 patient, angiotensin-converting enzyme inhibitor or angiotensin II receptor blockade in 5, calcium antagonist in 1, α-blocker in 2, diuretics in 4, anti-arrhythmic drug in 1 and nitrate in 1; those for HCM patients were β-blocker in 10 patients, angiotensin-converting enzyme inhibitor or angiotensin II receptor blockade in 5, calcium antagonist in 3, diuretics in 2, anti-arrhythmic drug in 2, and nitrate in 1. The control group consisted of healthy volunteers without any clinical or echocardiographic evidence of cardiovascular disease.

This study was approved both by the Research Ethics Committee of Hokkaido University Hospital and by the Ethics Committee of Faculty of Health Sciences in Hokkaido University.

Basic echocardiographic measurements

Echocardiography was performed using a Vivid 7 ultrasonographic machine (GE Healthcare UK Ltd, Amersham Place, Little Chalfont, Buckinghamshire, England) with an M4S transducer. The LV end-diastolic dimension and left atrial end-systolic dimension were measured from a parasternal long-axis B-mode image. The thicknesses of the IS and LV posterior wall were measured in the parasternal short-axis image at the level of the chordate tendineae at end-diastole. The LV ejection fraction was calculated by Simpson's biplane method of discs according to the American Society of Echocardiography.[14] Pulsed-Doppler echocardiography was performed to measure peak early and late diastolic transmitral flow velocities (*E* and *A*, respectively, cm/s) and the early diastolic wave deceleration time (DT, ms) of the transmitral flow and to calculate the ratio of early to late transmitral flow velocities (*E*/*A*). LV isovolumic relaxation time (IRT, ms) was measured using an apical continuous-wave Doppler recording, which

Figure 1 Measurement of mitral annular velocity using colour tissue Doppler imaging. In the apical four-chamber view (left panel), the peak early diastolic and peak late diastolic mitral annular velocities (e′ and *a*′, respectively) were measured at the interventricular septal (IS) and lateral wall (LW) side annulus (right panel).

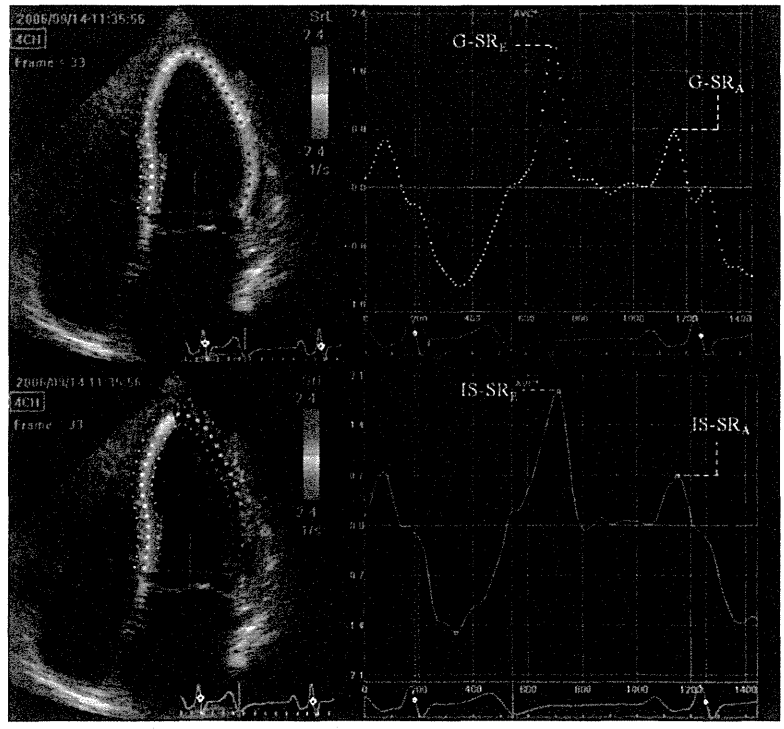

Figure 2 Measurement of myocardial strain rates using two-dimensional speckle-tracking imaging. Left ventricular global strain rates (upper panels): a region of interest for speckle-tracking analysis was set on the entire left ventricular myocardium in the apical four-chamber view (left panel). The peak early diastolic and late diastolic myocardial global strain rates (G-SR$_E$ and G-SR$_A$, respectively) were measured (right panel). The interventricular septal strain rates (lower panels): a region of interest was set on the interventricular septum from the base to the apex (left panel), and the peak early diastolic and late diastolic interventricular septal strain rates (IS-SR$_E$ and IS-SR$_A$, respectively) were measured (right panels).

clearly depicted both LV inflow and outflow. LV early diastolic flow propagation velocity (FPV, cm/s) was measured using apical colour M-mode Doppler imaging of the LV inflow along with the previously reported method.[15,16]

Measurement of mitral annular velocity by tissue Doppler imaging

An apical four-chamber image of the colour tissue Doppler technique was acquired at a frame rate of 69.8–147.7 frames/s. Tissue Doppler digital data were stored and analysed offline using an EchoPAC PC (GE Healthcare UK Ltd) (*Figure 1*). We measured the peak early diastolic and late diastolic velocity (e' and a', respectively, cm/s) at the mitral annuli of the IS and lateral wall (LW) sides and calculated the ratio of early to late diastolic annular velocities (e'/a'). The mean value of the two-site measurements (*M*-e', *M*-a', and *M*-e'/a') was also calculated for each study subject.

Measurement of strain rate by two-dimensional speckle-tracking imaging

Two-dimensional harmonic images (transmit/receive 1.9/4.0 MHz) in a four-chamber view were scanned with frame rates of 49–69/s. Digital data were stored and analysed offline using an EchoPAC PC (*Figure 2*). The LV endocardial surface of the end-systolic frame was traced manually, and the speckle-tracking width was modified so as to cover the whole LV wall thickness to obtain a so-called 'global' strain rate curve. From that curve, the peak early diastolic and late diastolic longitudinal strain rates (G-SR$_E$ and G-SR$_A$, respectively, S^{-1}) were measured. Then, the basal IS region of interest (ROI) was extended towards the apex, and the strain rate curve of the whole IS was obtained to measure the peak early diastolic and late diastolic IS strain rates (IS-SR$_E$ and IS-SR$_A$, respectively, S^{-1}). In a similar manner, a strain rate curve for the whole LW was obtained, and the two peak strain rates were measured (LW-SR$_E$ and LW-SR$_A$, S^{-1}). In addition, the ratio of the early to late diastolic peak was calculated each for the global, interventricular, and lateral strain rates (G-SR$_E$/SR$_A$, IS-SR$_E$/SR$_A$, and LW-SR$_E$/SR$_A$). Success or failure of the tracking was determined chiefly based on visual inspection of the tracking motion image, referring to the results of the automatic judgement function of the software, and manual readjustments were made if needed. Subjects for whom tracking was not completely successful were excluded from the study. All strain rates were expressed as absolute values.

Statistical analysis

Statistical analysis was performed using standard statistical software (Stat View version 5.0, SAS Institute, Cary, NC, USA). All numerical data were represented as means ± standard deviation. Differences among the three groups were tested by one-way analysis of variance at first, and, when a significant difference was detected, each difference

Table 1 Clinical characteristics and echocardiographic features

	Control ($n = 19$)	HT ($n = 13$)	HCM ($n = 15$)
Age (years)	52.6 ± 9.2	52.2 ± 12.5	54.3 ± 14.5
Male (%)	11 (58%)	7 (54%)	11 (73%)
Body surface area (cm^2)	1.69 ± 0.16	1.62 ± 0.23	1.69 ± 0.20
Heart rate (bpm)	62.3 ± 8.7	63.7 ± 8.6	59.6 ± 8.8
Systolic blood pressure (mmHg)	118 ± 11	132 ± 18**	115 ± 14††
Diastolic blood pressure (mmHg)	73 ± 8	82 ± 13*	67 ± 11†††
LV end-diastolic dimension (mm)	48.1 ± 2.9	46.2 ± 2.7	46.6 ± 5.8
LA end-systolic dimension (mm)	34.4 ± 4.2	37.6 ± 4.4	43.7 ± 7.0***††
Interventricular septal thickness (mm)	9.2 ± 1.4	13.3 ± 1.3**	20.4 ± 5.5***†††
LV posterior wall thickness (mm)	8.6 ± 1.3	11.4 ± 0.5***	10.2 ± 1.1***††
LV ejection fraction (%)	67.3 ± 4.8	66.5 ± 4.2	70.6 ± 8.5
E (cm/s)	77.9 ± 17.2	68.5 ± 14.8	69.3 ± 20.0
A (cm/s)	65.2 ± 12.3	71.6 ± 13.7	73.0 ± 23.2
E/A	1.26 ± 0.45	0.99 ± 0.28	1.09 ± 0.66
DT (ms)	193 ± 34	224 ± 34	261 ± 82***
IRT (ms)	77.6 ± 9.4	92.3 ± 11.4**	90.0 ± 20.6*
FPV (cm/s)	55.5 ± 8.7	45.5 ± 8.6**	37.5 ± 12.6***†
IS-*e'* (cm/s)	7.05 ± 1.67	4.39 ± 1.67***	3.48 ± 2.32***
LW-*e'* (cm/s)	9.06 ± 1.84	5.88 ± 1.62***	5.21 ± 3.18***
M-*e'* (cm/s)	8.06 ± 1.62	5.13 ± 1.55***	4.34 ± 2.69***
IS-SR_E (S^{-1})	1.37 ± 0.31	1.00 ± 0.28**	0.62 ± 0.41***††
LW-SR_E (S^{-1})	1.71 ± 0.36	1.12 ± 0.38***	0.89 ± 0.47***
Global-SR_E (S^{-1})	1.52 ± 0.35	1.03 ± 0.32***	0.70 ± 0.39***†

HT, hypertension; HCM, hypertrophic cardiomyopathy; LV, left ventricle; LA, left atrium; *E*, peak early diastolic transmitral flow velocity; *A*, peak late diastolic transmitral flow velocity; *E/A*, ratio of *E* to *A*; DT, early diastolic wave deceleration time of the transmitral flow; FPV, LV early diastolic flow propagation velocity; IRT, LV isovolumic relaxation time; *e'*, peak early diastolic mitral annular velocity; IS, interventricular septum; LW, lateral wall; *M*-*e'*, the mean value of IS-*e'* and LW-*e'*; SR_E, peak early diastolic strain rate.
*$P < 0.05$, **$P < 0.01$, ***$P < 0.001$ vs. control.$^{\dagger}P < 0.05$, $^{\dagger\dagger}P < 0.01$, $^{\dagger\dagger\dagger}P < 0.001$ vs. HT-LVH.

between the individual two groups was tested using a *post hoc* test. The relationship between two parameters was examined using linear correlation and regression analysis. The significance of the difference between two correlation coefficients was calculated using Fisher's *r*-to-*z* transformation. For all statistical tests, a *P*–value of <0.05 was used to indicate significance.

Results

Clinical background and echocardiographic parameters

There were no significant differences among the control, HT, and HCM groups in age, sex, heart rate, body surface area, LV end-diastolic dimension, LV ejection fraction, *E*, *A*, and *E/A* (*Table 1*). Systolic blood pressure and diastolic blood pressure were significantly greater in the HT group compared with the control or HCM group. IS thickness, LV posterior wall thickness, and IRT were significantly greater, and FPV was significantly reduced in both the HT and HCM groups compared with the control group. The left atrial dimension and DT were greater in the HCM group compared with the control group. The left atrial dimension and IS thickness were significantly greater, and FPV and LV posterior wall thickness were significantly lower in the HCM group than in the HT group. IS-*e'*, LW-*e'*, *M*-*e'*, IS-SR_E, LW-SR_E, and G-SR_E were significantly reduced both in the HT group and in the HCM group compared with the control group. IS-SR_E and G-SR_E were significantly reduced in the HCM group compared with the HT group.

Relationship between mitral annular velocities and strain rates of the corresponding wall

IS-*e'* was significantly and well correlated with IS-SR_E ($r = 0.90$, $P < 0.001$) (*Figure 3*). LW-*e'* was significantly, but less strongly, correlated with LW-SR_E ($r = 0.75$, $P < 0.001$). The correlation coefficient between IS-*e'* and IS-SR_E was significantly higher than that between LW-*e'* and LW-SR_E ($P < 0.05$). Significant and good correlation was also observed both between IS-*e'*/*a'* and IS-SR_E/SR_A ($r = 0.88$, $P < 0.001$) and between LW-*e'*/*a'* and LW-SR_E/SR_A ($r = 0.84$, $P < 0.001$).

Relationship between mitral annular velocities and left ventricular global strain rate

IS-*e'* and *M*-*e'* were significantly and well correlated with G-SR_E ($r = 0.88$, $P < 0.001$ and $r = 0.86$, $P < 0.001$, respectively) (*Figure 4*). IS-*e'*/*a'* and *M*-*e'*/*a'* were also well correlated with